Journal of Geochemical Exploration 182 (2017) 32–52

Contents lists available at ScienceDirect

Journal of Geochemical Exploration

journal homepage: www.elsevier.com/locate/gexplo

Formation of the Eğrikar (Gümüşhane) Fe–Cu skarn type mineralization in NE Turkey: U–Pb zircon age, lithogeochemistry, mineral chemistry, fluid inclusion, and O-H-C-S isotopic compositions

Ferkan Sipahi*, İbrahim Akpınar, Çiğdem Saydam Eker, Abdullah Kaygusuz, Alaaddin Vural, Meltem Yılmaz

Department of Geological Engineering, Gümüşhane University, TR-29000 Gümüşhane, Turkey

ARTICLE INFO

Keywords:
Fe–Cu skarn
Fluid inclusion
Geochemistry
Stable isotope
Turkey
U–Pb zircon age

ABSTRACT

The Eğrikar Fe–Cu skarn type mineralization is located approximately 100 km NW of Gümüşhane in NE Turkey. Geochemical analyses of diorite, which is thought to cause skarn, indicate medium K calc-alkaline (1.3 to ~2.3 wt % K_2O), metaluminous to peraluminous (A/CNK = 0.76 to 1.13) and resembles a continental arc granite. The age of U–Pb zircon obtained from diorite is 42.3 ± 1.0 Ma, which reflects the age of skarn metasomatism after intrusion into Late Cretaceous sandy carbonates. Skarn formation zones are recognized as *endo*- and exoskarn. The endoskarn zone mainly consists of pyroxene with hedenbergite ($Di_{4.31–28.14}Hd_{59.29–80.82}Jo_{5.0–35.55}$) at prograde stage. Mn content of pyroxene increases a slight from endo to exoskarn. Pyroxene is replaced by epidote and hornblende at the retrograde stage. The exoskarn zone comprises garnet with andradite ($Ad_{91-99}Gr_{01–07}$) and grossular-andradite ($Ad_{44-95}Gr_{05–54}$), epidote and quartz as silicate minerals, and magnetite and hematite as ore minerals. Magnetite is the abundant ore mineral and is accompanied by chalcopyrite and minor pyrite at retrograde stage.

On the basis of fluid inclusion values of minerals, the temperature range for hedenbergite in *endo*-exoskarn is 350 °C–425 °C, for epidote in exoskarn is 365 °C–376 °C, and for quartz in exoskarn 200 °C–380 °C. NaCl equivalent salinity for hedenbergite 6.88–10.73 wt% and for quartz is 3.9–15.38 wt. The $\delta^{18}O$ values of hedenbergite is 4.1 to 4.7‰ and for garnet 3.4‰ at prograde stage, for epidote 7.9–9.2‰, for magnetite 1 to 4.4‰, for hematite − 2.9 to − 1.6‰ and for quartz range between 8.5‰ and 15.2‰. The $\delta^{18}O$ value of epidote suggests that oxygen is a magmatic fluid whereas hedenbergite, garnet, quartz and magnetite show the mixing of magmatic and meteoric fluids. In addition, the C isotope values (− 3.2 to 2.8‰) of calcite and marble in Eğrikar Fe–Cu skarn reflect those of metamorphic, and skarns. Based on oxygen isotope data from mineral pairs, the retrograde skarn formation is characterized by epidote–magnetite assemblage formed at 255 °C–438 °C. Fluid oxygen isotope compositions of magnetite and epidote pairs of the exoskarn skarn zone indicate a mixing of magmatic and meteoric fluids with narrow $\delta^{18}O$ values between 7.17‰ and 8.9‰. The $\delta^{34}S$ values of the pyrites exhibit a narrow range of 3‰ and 4.4‰, thereby indicating that sulfur were probably leached from magmatic rocks.

Based on the field and laboratory observation, mineral chemistries, fluid inclusion studies and isotope composition analysis, it is suggested that the Eğrikar Fe–Cu skarn mineralization occurs in a magmatic origin fluids being initially under reduced conditions, subsequently under oxidized conditions, and at shallow depth.

1. Introduction

The Eastern Black Sea Region of NE Turkey is a well-known metallogenic province (Pejatoviç, 1971; Aslaner et al., 1995) that contains numerous skarn, porphyry, and vein-type deposits related to Eocene or Late Cretaceous volcano–plutonic systems (Yiğit, 2006, 2009). Plutonic rocks (specifically Late Cretaceous and Eocene) in the region caused the formation of skarn deposits in carbonate rocks (Fig. 1). Saraç (2003) and Saraç and Van (2005) examined that the geochemical characteristics of granitoids related to the formation of skarn deposits in Çambaşı-Kabadüz (Ordu), Dereli (Giresun), Özdil (Trabzon), Arpalı (Trabzon), Ögene (Trabzon), and

* Corresponding author.
E-mail address: ferkansipahi@gumushane.edu.tr (F. Sipahi).

http://dx.doi.org/10.1016/j.gexplo.2017.08.006
Received 21 August 2016; Received in revised form 7 July 2017; Accepted 4 August 2017
Available online 07 August 2017

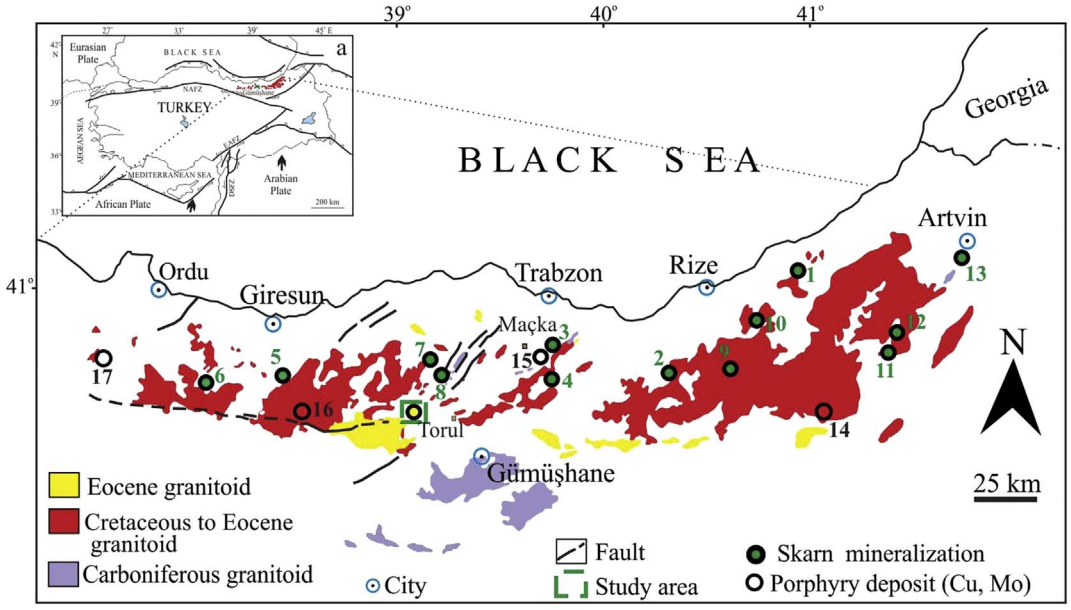

Fig. 1. a) Tectonic map of Turkey (modified after Şengör et al., 2003) and b) Simplified geological map showing the various granitoids and skarn deposits distributions in the eastern Black Sea region (modified after MTA, 2002). 1. Kartiba, 2. Ögene, 3. Özdil, 4. Camiboğazı-Arnastal, 5. Dereli, 6. Çambaşı, 7. Sekü, 8. Donguldere, 9. İkizdere, 10. Ovit Dağı, 11. Dokumacılar, 12.Çıkacor, 13. Demirköy, 14. İspir-Ulutaş, 15. Güzelyayla, 16. Emeksen, 17. İlbeyli.

Kartiba (Rize) Fe Skarn deposits exhibit I-type, calc-alkaline, and metaluminous to peraluminous transitional properties of arc granitoids. The Arnastal Fe skarn and Camiboğazı skarn in Gümüşhane were formed under oxidized conditions as a result of contact pyrometasomatic activities related to I-type, high K calc-alkaline, and metaluminous Late Cretaceous granitoid (Sipahi, 2011). Skarn deposits have been studied in the Gümüşhane area by Takaoğlu et al. (1978), Çekiç et al. (1985) and Er and Serdar (1992). The Eğrikar Fe–Cu mineralization is located at approximately 100 km NW of Gümüşhane in the Eastern Black Sea Region of Turkey and an old mine. In unknown date, Eğrikar mine produces iron ore. The MTA (Mineral Research and Exploration General Directorate of Turkey) estimated grades of 9.29%–47.78% Fe and 0.14%–11.26% Cu (Çekiç et al., 1985). Er and Serdar (1992) determined that Eğrikar mineralization covers an area of 700 m × 300 m and includes pyrite, magnetite, and chalcopyrite, with mean grades of 0.8% Cu.

In the Eğrikar area of the Gümüşhane in the Eastern Black Sea Region of NE Turkey, arc-related magmatism developed under a compressional regime and is characterized by the predominance of calc-alkaline granitoids (Sipahi et al., 2016). Prior to the present research, knowledge about the geochronological age, petrography, lithogeochemistry, mineral chemistry, and isotopic composition of the Eğrikar Fe–Cu skarn mineralization is not known. In the present study, the geology, lithogeochemistry, mineral chemistry, fluid inclusion, and O-H-C-S isotopic characteristics of the Eğrikar Fe–Cu skarn mineralization are described in detail. This study aims to describe the geological and geochemical aspects of the Eğrikar Fe–Cu skarn mineralization in terms of mineral chemistry, paragenesis, geochemistry (analysis of whole rock, trace element, and rare earth element (REE) in rocks), stable isotopes ($\delta^{18}O$, $\delta^{13}C$, δD, and $\delta^{34}S$), and U–Pb zircon age isotope of diorite. These data are used to examine the formation of Eğrikar Fe–Cu skarn mineralization.

2. Regional geology

The study area is located in the Eastern Black Sea region of NE Turkey; the Eastern Black Sea region is developing as a continental magmatic arc, block-faulted tectonic formation with subduction involved in the settlement of granitic plutons from the Carboniferous to the Eocene periods during subduction of the Tethyan oceanic crust (Gedikoğlu, 1979; Şengör and Yılmaz, 1981). Late Jurassic granitoids are commented as the products of an arc-continent collision event, in response to closure of the Paleotethys during the middle Jurassic and the accretion of the Sakarya block to Laurasia in the north (Şengör and Yılmaz, 1981; Yılmaz et al., 1997; Dokuz et al., 2010). During the Late Cretaceous, arc-type volcanics and intrusive rocks were emplaced into the Eastern Pontide crust in response to northward subduction of the Neotethyan oceanic crust beneath the Eurasian plate (Şengör and Yılmaz, 1981; Okay and Şahintürk, 1997; Yılmaz et al., 1997; Okay and Tüysüz, 1999; Şengör et al., 2003; Topuz et al., 2007; Altherr et al., 2008; Ustaömer and Robertson, 2010). Late Cretaceous arc type volcanic rocks mainly belong to the tholeiitic and calc-alkaline series, which display typical island arc characteristics (Çamur et al., 1996; Arslan et al., 1997; Sipahi and Sadıklar, 2014; Sipahi et al., 2014). The Paleocene time in the region shows to a continent-continent collision between the Pontides magmatic arc and the Tauride-Anatolide block due to the closure of the Neotethys (Okay and Şahintürk, 1997; Boztuğ et al., 2004). It is proposed a Paleocene to early Eocene collision, causing crustal thickening (Şengör and Yılmaz, 1981; Okay and Şahintürk, 1997). The collision occurring in the late Paleocene to early Eocene based on field relationships and granitoid ages were suggested by Okay et al. (1997). Early Eocene adakitic rocks, have been reported in the region showing a *syn-* to post-collision phase (Topuz et al., 2005; Eyüboğlu et al., 2011). The Middle Eocene time includes a large belt of E–W trending volcanic (Tokel, 1977; Şen et al., 1998) and granitoid rocks (Yılmaz and Boztuğ, 1996; Boztuğ et al., 2004) towards Iran and the Caucasus. The Middle Eocene volcanic and volcanoclastic rocks are intruded by calc-alkaline granitoids of similar ages (Arslan and Aslan, 2006).

Numerous researchers (e.g., Moore et al., 1980; Aslaner et al., 1995; Sipahi and Sadıklar, 2010; Sipahi, 2011; Akaryalı, 2016; Akaryalı and Akbulut, 2016) investigated ore deposits of Gümüşhane area at the Eastern Black Sea Region. However, studies on granitoids (Eğrikar Monzogranite and Erik Granitoid) and Fe–Cu skarn mineralization in Eğrikar area are limited and primarily focused mines, including general geological research (Çekiç et al., 1985; Er and Serdar, 1992; Güven, 1993; Yılmaz, 2016). This study

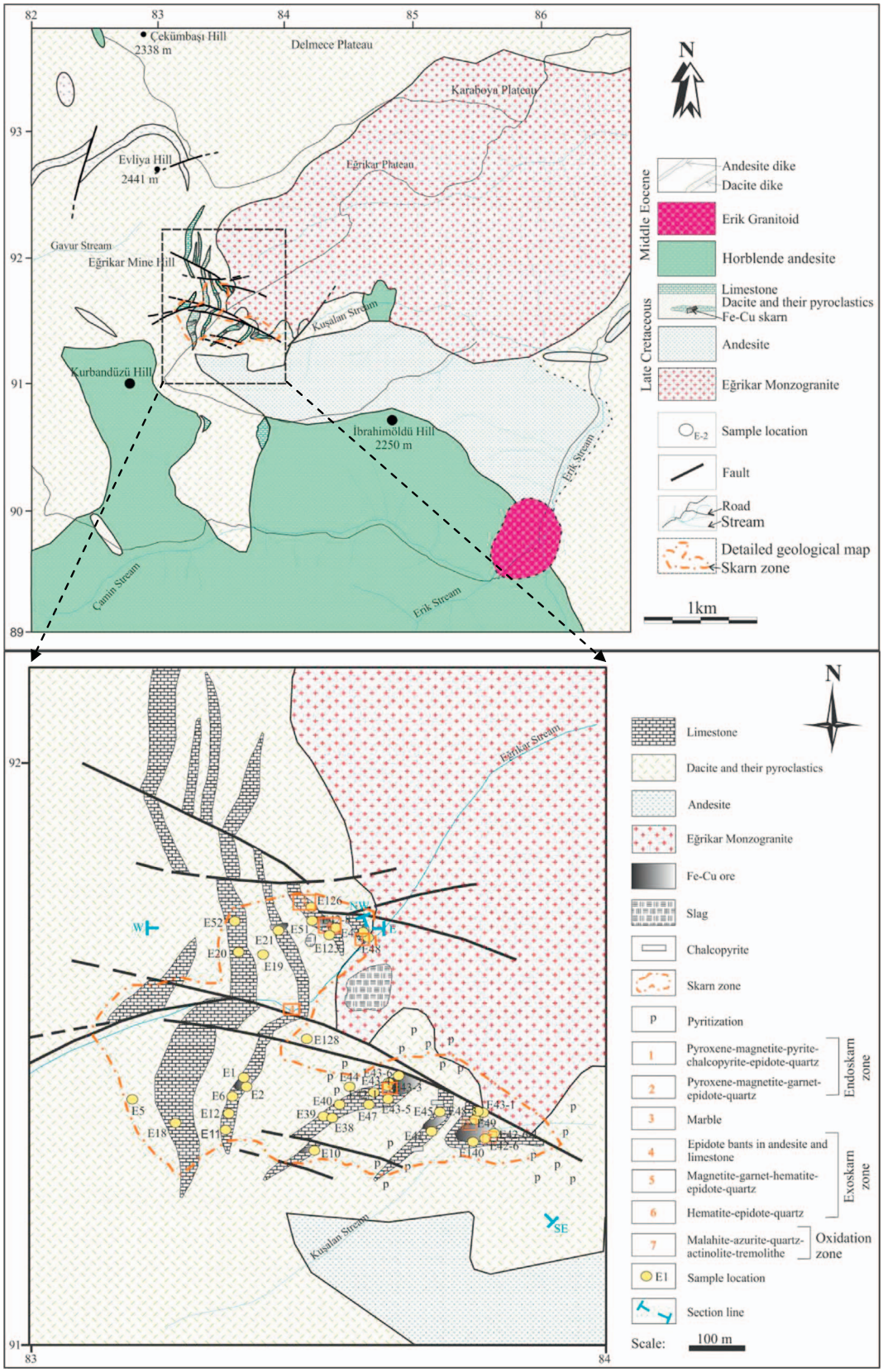

Fig. 2. The geological map of the Eğrikar Fe-Cu skarn mineralization.

explains the formation of the Eğrikar Fe–Cu skarn mineralization with mineral chemistry, fluid inclusion, stable (O-, H-, C- and S-) isotope composition properties and lithogeochemistries of granitoid and limestone in the Eğrikar area. In addition, this article reports geochemical and U–Pb zircon ages from the Eğrikar Monzogranite (80.5 ± 1.7 Ma) and Erik Granitoid (42.3 ± 1.0 Ma) in the Eğrikar

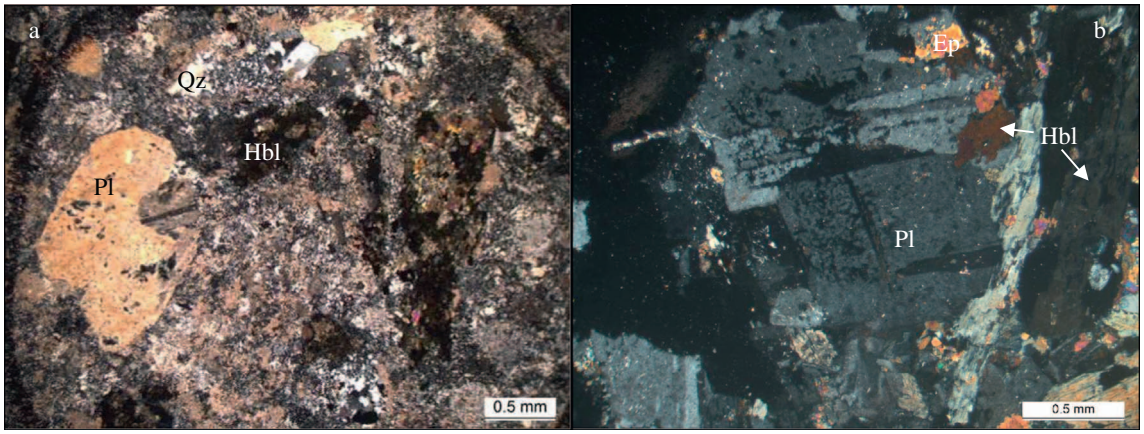

Fig. 3. The textures of the Erik Granitoid. a) Granular texture in the granodiorite (sample number: E-139) and b) Hornblende and plagioclase in diorite (sample number: E-120A), Pl: Plagioclase, Hbl: Hornblende, Qz: Quartz, Ep: Epidote.

area. The basement of the study area is made up of a Campanian Eğrikar Monzogranite. The basement rocks are overlain by the Late Cretaceous aged volcano-sedimentary units consist of dacite and their pyroclastics, including sandy limestone, limestone strata, and hornblende andesite in the study area (Fig. 2). The age of the limestone has been accepted as Middle-Upper Maastrichtian based on paleontological (*Rosita contusa* (Cushman), *Gansserina gansseri* (Bolli), *Globotruncana* cf. *bulloides* Vogler, *Globotruncanita* cf. *conica* (White) and *Globotruncana ventricosa* (White)) evidence. The calc-alkaline I-type Erik Granitoid, consisting of granodiorite and diorite, is observed into sourthern east part of the Eğrikar area in the Eastern Pontides and cause the Eğrikar Fe-Cu skarn mineralization into the Late Cretaceous volcano-sedimentary unit during the Middle Eocene time. Eğrikar (Gümüşhane, NE Turkey) Fe–Cu skarn mineralization developed at the Middle-Upper Maastrichtian aged limestone.

3. Methodology

3.1. Whole-rock geochemical analyses

Twenty samples were obtained from granitoids in the Eğrikar. The modal mineralogies of these samples were determined through point counting using a Swift automatic counter fitted to a polarizing microscope in Gümüşhane University, Department of Geological Engineering. Based on microscopic studies, 12 fresh (or least altered) and more representative samples were selected for analysis of major, trace, and REE in the commercial ACME Laboratories, Ltd. (Vancouver, Canada). Major elements were identified by inductively coupled plasma–atomic emission spectrometry after fusion with $LiBO_2$. About 0.2 g of the sample powder and 1.5 g of $LiBO_2$ flux were mixed in a graphite crucible and heated to 1050 °C for 15 min for analysis of trace elements and REE. The detection limits were set within 0.01 wt%–0.1 wt% for major oxides, 0.1–10 ppm for trace elements, and 0.01–0.5 ppm for REEs.

3.2. U–Pb zircon age dating analyses

U–Pb zircon age dating was performed using LA–ICP–MS at the Geologic Laboratory Center, China University of Geosciences (Beijing, China). Zircon grains for U–Pb dating were extracted using heavy liquid and magnetic separation and then purified by hand picking under a binocular microscope. The selected grains were mounted on an epoxy resin and polished half-way. Cathodoluminescence images were used to examine the zoning and internal structures of individual zircon grains and to select a better spot for analytical positions. A quadrupole ICP–MS apparatus (Agilent 7500a) was connected to UP-193 solid-state laser (193 nm, New Wave Research Inc.) with an automatic positioning system. Laser spot size, energy density, and repetition rate were set to approximately 36 μm, 8.5 J/cm^2, and 10 Hz, respectively. The ablated material was transferred into ICP–MS equipment by a high-purity He gas stream with a flux of 0.8 L/min. The U–Pb isotopic fractionation effects were corrected using zircon 91,500 (Wiedenbeck et al., 1995) as external standard. The zircon standard TEMORA (417 Ma, Black et al., 2003) was also used as a secondary standard to monitor the deviation of age measurement/calculation. A total of 10 analyses of TEMORA showed the apparent $^{206}Pb/^{238}U$ ages of 417–418 Ma. The isotopic ratios and elemental concentrations of zircon were calculated using GLITTER software (ver. 4.4, Macquarie University). Uncertainties on age data are given as 1 sigma level. Concordia ages and diagrams were prepared using Isoplot/Ex (3.0) (Ludwig, 2003). Common lead was corrected following the method of Andersen (2002).

3.3. Mineral chemistry analyses

Compositions of skarn minerals were determined using a Cameca SX-100 electron microprobe with three wavelength dispersive spectrometers at the New Mexico Institute of Mining and Technology (Socorro, New Mexico, USA). Spot analyses were conducted under operating conditions of 15 kV accelerating voltage, beam current of 20 nA, and beam diameter of 10 μm. The samples were examined using backscattered electron imagery and quantitatively analyzed. Kaersutite (UCB), diopside (UCB), orthoclase (UCB), and magnetite (UCB) were used as standard reference materials.

3.4. Fluid inclusion analyses

Fluid inclusion measurements were carried out using double polished thick sections at the Central Research Laboratory of Gümüşhane University (Turkey). The investigations were conducted at − 196 °C to 600 °C, with a measurement accuracy of ± 0.2 °C within + 200 °C to − 20 °C; beyond this range, the accuracy was ± 1.5–2 °C.

3.5. Stable isotope analyses

Oxygen, hydrogen, carbon, and sulfur isotopes were analyzed at the Queen's Facility for Isotope Research (QFIR, Canada). Hedenbergite, garnet and magnetite were analyzed for $\delta^{18}O$ value, amphibole and epidote for $\delta^{18}O$ and δD values, calcite for $\delta^{13}C$ and

Table 1
Whole-rock analyses of the Erik Granitoid and carbonate rocks from Eğrikar Fe-Cu skarn mineralization.

Sample number	Erik Granitoid			Limestone	Crystallized limestone	Marble
	Granodiorite	Diorite				
	E-139	E-120A	E-138C	E52	E126	E29
SiO_2	65.77	52.04	57.67	20.69	14.12	40.92
TiO_2	0.34	0.64	0.57	0.02	0.02	0.28
Al_2O_3	15.47	15.91	17.46	3.53	2.35	7.71
Fe_2O_{3t}	4.08	8.04	6.62	0.49	0.32	3.55
MnO	0.08	0.17	0.08	0.04	0.03	0.12
MgO	1.98	7.78	3.05	0.79	0.50	2.03
CaO	2.65	7.55	5.58	39.40	44.65	23.50
Na_2O	3.87	3.47	3.03	0.49	0.05	0.45
K_2O	2.27	1.30	2.32	0.84	0.69	1.28
P_2O_5	0.12	0.11	0.18	< 0.01	0.01	0.14
Cr_2O_3	0.003	0.042	0.005	< 0.002	< 0.002	0.003
LOI	3.20	2.70	3.10	33.60	37.10	19.90
Total	99.77	99.75	99.68	99.89	99.88	99.86
Tot. C	0.22	0.07	0.04	8.72	10.27	4.85
Tot. S	< 0.02	< 0.02	< 0.02	< 0.02	0.03	0.13
Ba	1014	640	634	172	167	270
Sc	10	30	16	< 1	< 1	8
Be	3	2	5	< 1	< 1	1
Co	9.3	29.7	14.2	0.7	1.1	4.2
Cs	0.5	< 0.1	0.4	0.3	0.3	1.2
Ga	12.7	17.1	15	2.6	1.9	7.1
Hf	2.3	1.9	2.4	0.7	0.5	2.2
Nb	4	2.7	3.7	2	1.1	4.3
Rb	42.7	28.6	65.6	28.1	19.8	40.8
Sn	< 1	< 1	< 1	< 1	< 1	1
Sr	267.1	606.6	645.6	519.7	611.4	317.4
Ta	0.3	< 0.1	0.3	0.2	0.2	0.3
Th	8.8	2.4	5.5	5.2	2.9	6.9
U	2.6	0.4	2	1.4	1.3	2.1
V	86	213	181	< 8	< 8	107
W	0.8	< 0.5	1.4	< 0.5	< 0.5	1.2
Zr	81.9	69.4	84.4	18.7	14.9	83
Y	9.5	17.7	15.7	5.9	3.6	12.1
Mo	3.5	1.7	2.7	1.1	0.7	1
Cu	7.2	3.8	544.7	2.2	5.7	14.9
Pb	5.9	0.7	3.7	12.6	54.3	31.4
Zn	21.0	20	35.0	4	30	33
Ni	10.7	52.9	11.4	0.5	1.6	10.8
As	0.6	1.1	0.9	1	0.8	4.8
Cd	< 0.1	< 0.1	0.1	< 0.1	0.2	< 0.1
Au	< 0.5	< 0.5	0.9	0.5	< 0.5	1.1
La	21.8	12.3	21.2	8.5	6.9	16.7
Ce	36.5	22.0	39.5	14.9	10.3	29.9
Pr	3.78	2.70	4.46	1.56	1.11	3.27
Nd	13.4	11.9	16.1	5.6	3.7	12.3
Sm	2.66	2.89	3.14	0.83	0.66	2.23
Eu	0.74	0.87	1.02	0.14	0.13	0.47
Gd	2.3	3.04	3.17	0.87	0.58	2.34
Tb	0.31	0.49	0.52	0.13	0.09	0.36
Dy	1.89	2.78	2.81	0.92	0.51	2.12
Ho	0.39	0.56	0.57	0.17	0.08	0.43
Er	1.03	1.74	1.72	0.54	0.27	1.30
Tm	0.19	0.25	0.26	0.09	0.05	0.20
Yb	1.2	1.58	1.74	0.59	0.29	1.31
Lu	0.21	0.24	0.26	0.09	0.05	0.19

$\delta^{18}O$ values, and pyrite for $\delta^{34}S$ value. All results were calibrated to certified reference materials reported in standard per mil notation (‰) and relative to the following international standards (VSMOW for $\delta^{2}H$, VSMOW for $\delta^{18}O$, VPDB for $\delta^{13}C$, and VCDT for $\delta^{34}S$). Accuracy reported (1.5‰ for $\delta^{2}H$, 0.5‰ for $\delta^{18}O$, 0.1‰ for $\delta^{13}C$, and 0.2‰ for $\delta^{34}S$) per mil notation (‰) is based on primary or secondary standard analyses.

4. Results

4.1. Petrography and geochemistry of Erik Granitoid

Erik Granitoid observing in SE of the Eğrikar area with medium granular texture is composed of plagioclase ($An_{38–48}$), hornblende, orthoclase, quartz, biotite, epidote, and opaque minerals (Fig. 3). Zircon occurs as an accessory mineral.

Erik Granitoid contains 52 wt%–65 wt% SiO_2 and 15 wt%–17 wt% Al_2O_3 (Table 1). The rock is classified as medium-K calc-alkaline (from 1.3 wt% to ~2.3 wt% K_2O) and peraluminous to metaluminous (A/CNK [molecular $Al_2O_3/(CaO + K_2O + Na_2O)$] is 0.76–1.13) (Sipahi et al., 2016; Fig. 4).

Erik Granitoid was formed in a magmatic arc-related environment based on its trace element concentrations. The trace element concentrations of Erik Granitoid are close to those of plutons associated with Fe and Cu skarn mineralization (Fig. 5).

4.2. Carbonate rocks

Carbonate rocks consist of sandy limestone and limestone, which occur as crystallized limestone and marble. High Ca and low Mg values are present in sandy limestone compared to the recrystallized limestone (Table 1). In the study area, the Ca and Mg values of the crystallized limestone are similar to those of the dolomitic marble (51% CaO and 3.09% MgO; Lentz and Suzuki, 2000). The CaO (or CO_2) value decreases by about 40%, whereas the MgO value increases by about 157% from sandy limestone to marble. This result is suitable to other calcic skarn mineralization (Barton et al., 1990; Lentz and Suzuki, 2000). The samples display high Al_2O_3/SiO_2 (0.166–0.188) ratio; such trace element enrichment is ascribed to hydrothermal activities (İstanbullu, 2013). In the diagrams of TiO_2 versus SiO_2/Al_2O_3, SiO_2 versus Fe_2O_{3t}, SiO_2 versus Ce, and Al_2O_3 versus Ce (Fig. 6), the limestone samples in the Eğrikar Fe–Cu skarn mineralization show strong correlations, which determine that carbonate disengagement actualizes at temperatures that can affect Al and Ce mobility (Leitch and Lentz, 1994).

4.3. Geology of skarn mineralization

The Eğrikar Fe–Cu skarn mineralization mainly occurs in limestones, whereas host rocks for skarns are identified as volcano-sedimentary rocks such as Çambaşı (Ordu), Dereli (Giresun) and Özdil (Trabzon) Fe-Cu skarn mineralizations in the Eastern Black Sea Region of NE Turkey. The Eğrikar Fe–Cu skarn mineralization area is generally fractured and distributed in the area where the old mining area is; this area consists of limestone lenses, ore mass, and skarn minerals (Figs. 7 and 8). The orebodies in the Eğrikar Fe–Cu skarn mineralization contain approximately 0.5 m × 1 m and 1 m × 1.5 m in size of magnetite, specular hematite, garnet, epidote, and quartz. The most important characteristic of this skarn mineralization is the formation of both poorly developed endoskarn and well-developed exoskarn.

In the Eğrikar Fe–Cu skarn mineralization, *endo-* and exoskarn zones developed from granitoid to limestone (Fig. 8). Endoskarn is represented by pyroxene in the Eğrikar Fe-Cu mineralization and magnetite and garnet are developed after pyroxene. Anhydrous and high-temperature minerals, such as pyroxene, magnetite and garnet in the Eğrikar Fe-Cu skarn mineralization, occurred at the prograde stage (Fig. 9a). Retrograde epidote, hornblende, calcite and a small amount of chlorite replaced pyroxenes and show transition to the exoskarn zone in the Eğrikar Fe-Cu skarn mineralization (Fig. 9a and b). Moreover, epidotes were found as replacing magnetite and

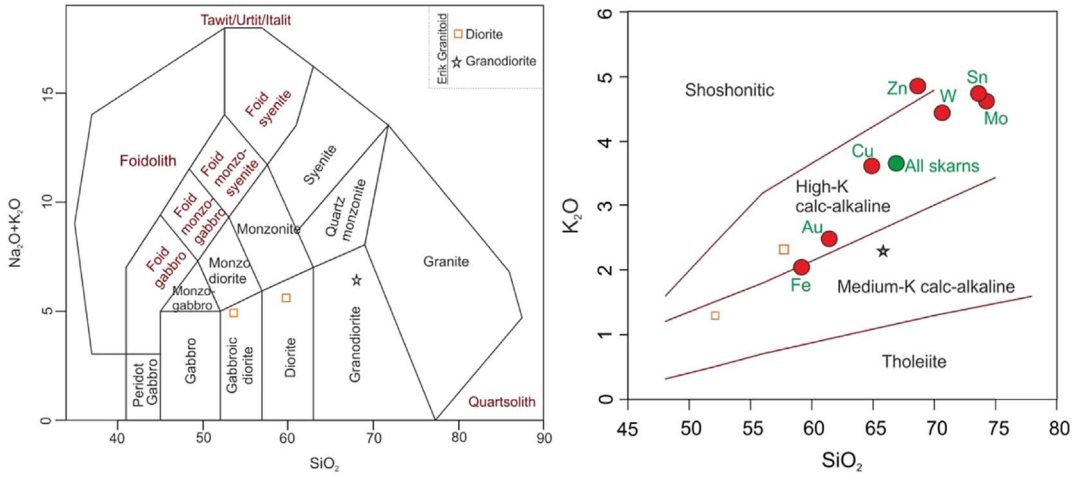

Fig. 4. a) SiO_2 vs $Na_2O + K_2O$ diagram (Middlemost, 1994) and b) SiO_2 vs K_2O (Le Maitre et al., 1989; data for plutonic rocks associated with main skarn deposits from Meinert et al., 2005) diagram showing variations of the Erik Granitoid samples in the Eğrikar Fe-Cu skarn mineralization.

garnet in the exoskarn zone of the Eğrikar Fe-Cu skarn mineralization. Epidotes were also observed as epidote veins in andesite and limestone, epidote spots in diorite, and around the radial hematite lenses in the study area. In addition, in this skarn mineralization, the spaces and fractures between garnets belonging to prograde are filled with hematite and quartz (Fig. 9c and d). Hydrous minerals, such as epidote, hornblende, and chlorite, developed at the retrograde stage (Einaudi and Burt, 1982; Meinert, 1992, 1997; Meinert et al., 2005; Orhan et al., 2010; Sipahi, 2011). Some epidotes generally grow along the fractures of pyroxene and garnet, belonging to the prograde stage (Einaudi, 1982; Murakami, 2005).

4.4. Skarn paragenesis

Magnetite, pyrite, hematite, and chalcopyrite (grade of 0.8% Cu; Er

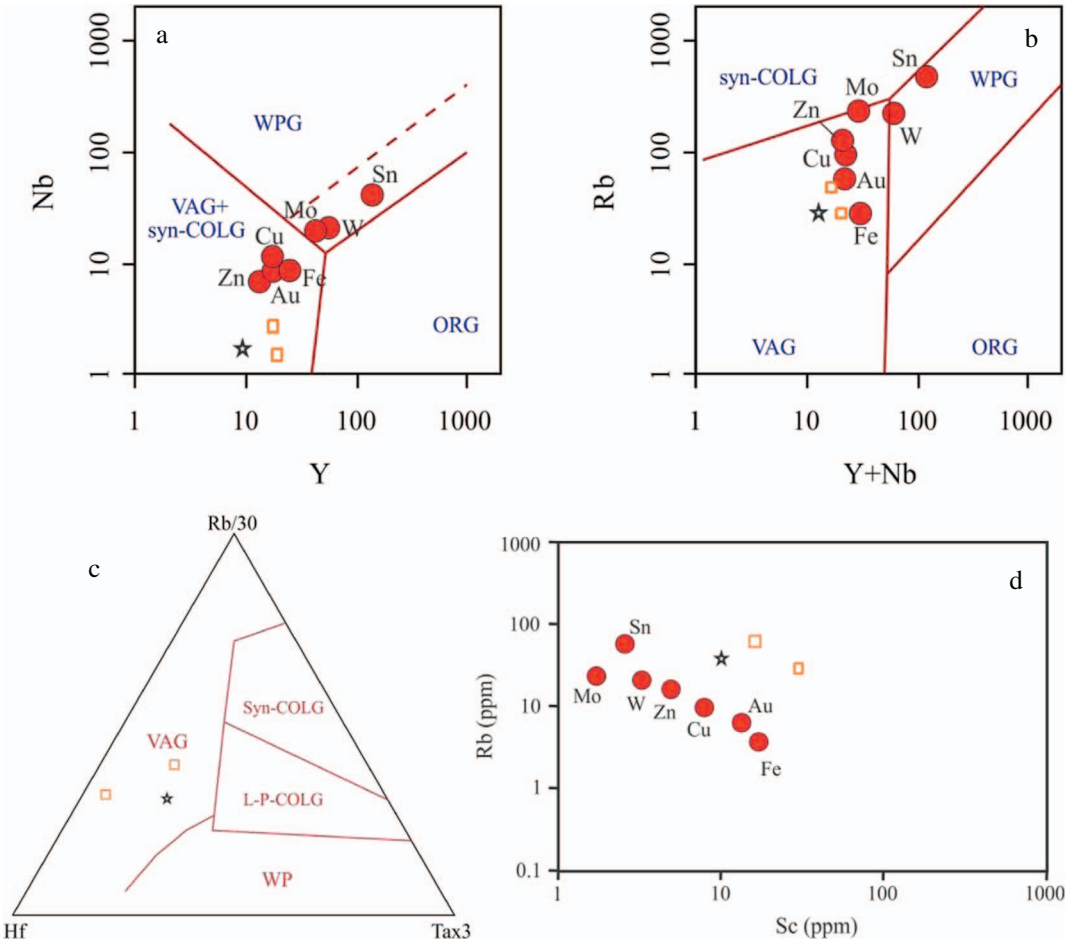

Fig. 5. a) Nb-Y and (b) Rb-(Y + Nb) diagrams (Pearce et al., 1984, data for plutonic rocks from Meinert, 1985), c) Rb-Ba-Sr ternary diagram (Ray et al., 2000; data for plutonic rocks including skarn from Ray et al., 1996) and d) Sc vs Rb diagram (Meinert, 1995; Meinert et al., 2005) showing variations of the Erik Granitoid samples. Symbols are the same as in Fig. 4.

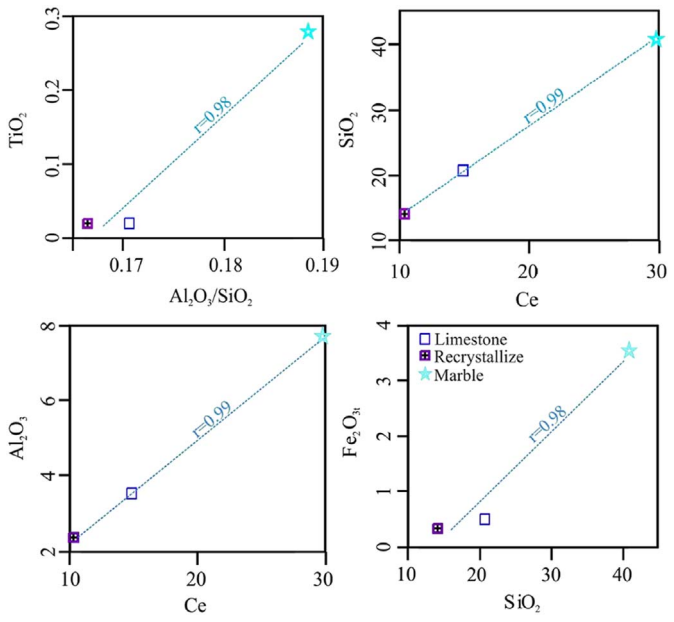

Fig. 6. a) SiO_2/Al_2O_3 vs TiO_2, b) Ce vs SiO_2, c) Ce vs Al_2O_3 diagrams and d) SiO_2 vs Fe_2O_{3t} diagram showing variations of limestones from Eğrikar Fe—Cu skarn mineralization.

and Serdar, 1992) are abundant ore minerals (Table 2). Alteration and oxidation minerals include hematite, goethite, digenite, malachite, azurite, covelline, bornite, and lepidocrocite. Magnetite and pyrite follow as an early ore phase. Chalcopyrite is formed after pyrite. Some magnetites are replaced with hematite (Fig. 10a). Some pyrites have cataclastic texture showing a deformation or fluid-pressure (Fig. 10b). Magnetite which is generally xenomorph and subotomorph is massive. Hematite replaced some pyrites. Hematite develops radial and lattice (Fig. 10c). Martite develops along some magnetite crystal edges and fractures. Some magnetites include small chalcopyrite inclusions (Fig. 10d). Chalcopyrite find as an inclusion in the gangue (Fig. 10b). Covelline, bornite, and digenite developed in the chalcopyrite fractures. Quartz is associated with magnetite and hematite. Supergene effects include replacement of chalcopyrite, pyrite, and hematite with malachite, azurite, covelline, bornite, and goethite.

4.5. Skarn and ore mineralogy

In Eğrikar Fe–Cu skarn mineralization, EPMA was utilized to determine skarn mineral types and chemistry of the ore minerals. The chemical analysis results of pyroxene, garnet, epidote, magnetite, chalcopyrite, and pyrite for Eğrikar Fe–Cu skarn mineralization are shown in Table 3.

Pyroxene is associated with less magnetite, chalcopyrite, epidote, and quartz in samples from the endoskarn zone of Eğrikar Fe–Cu skarn mineralization. In this zone, epidote replaces some pyroxenes. Magnetite was observed between pyroxenes. MnO in pyroxene ranges from 1.53% to 9.58% and shows high values (Table 3). In Eğrikar Fe–Cu skarn mineralization, pyroxene with low Mn content is associated with less amount of chalcopyrite in the endoskarn zone. The Mn/Fe values of pyroxene from Eğrikar Fe–Cu skarn mineralization are generally < 0.15 and show similarity to the Cu-Fe skarn-type deposit. Al_2O_3 content in pyroxene changes from 0.05% to 0.26%. The pyroxene type in Eğrikar Fe–Cu skarn mineralization is hedenbergite ($Di_{4.31–28.14}Hd_{59.29–80.82}Jo_{5.0–35.55}$) and shows less diopside and johannsenite (Fig. 11). The Mg, Mn, and Fe contents of pyroxenes change compare to skarn types, and some Fe skarn deposits contain high amounts of johannsenite-bearing pyroxene (Einaudi and Burt, 1982; Matsueda, 1981). Einaudi and Burt (1982) reported that the Mn content in pyroxene from the Fe skarn is higher than that in the Cu skarn but lower than that in the Pb-Zn skarn. Nakano et al. (1994) and Nakano (1998) determined that pyroxenes exhibit different Mn/Fe values in different skarn types and suggested < 0 0.14 for Cu-Fe type and > 0.2 for Pb-Zn type. The Mn/Fe ratio of pyroxene from the Ayazmant (Balıkesir, Turkey) Fe–Cu skarn deposit ranges from 0.005 to 0.02 and is low (Oyman, 2010). Nakano et al. (1994) determined that the Al_2O_3 content of pyroxene in skarns is generally below 1%. Some researchers (Einaudi et al., 1981; Nakano et al., 1994) determined a relationship exists between the skarn mineral composition and skarn deposit metal contents; they also showed that johannsenite develops in Zn-skarns and diopsite–hedenbergite in Fe–Cu skarns.

Garnet is observed otomorph–subotomorph and shows isotropic and anisotropic properties. Garnet shows zoning, such as thin bands, and cataclastic texture in some samples. Garnet is partly replaced with quartz-Fe-oxide-epidote and remains as a relic in some samples. Some garnet was also observed together with hematite. The type of garnet is andradite ($Ad_{91-99}Gr_{01–07}$) in *endo*-exoskarn transitional zone and grossular-andradite ($Ad_{44-95}Gr_{05–54}$) in the exoskarn zone (Fig. 12). Fe^{2+} is dominant in garnet (garnet 1) of the endo- and exoskarn transitional zones, whereas Fe^{3+} is dominant in the garnet (garnet 2) from the exoskarn zone. Zoning garnet is composed of grossular-andradite. In general, the Ad/Gr ratio of garnet increases in the exoskarn zone from Eğrikar Fe–Cu skarn mineralization. Abu El-Enen et al. (2004) expressed that the increase in Ad/Gr ratio from the core to the rim of garnet is related to the oxidized degree of $f(O_2)$, and the Ad/Gr ratio increases with increasing of $f(O_2)$.

Epidote was observed in hornblende andesite and in limestone with garnet, magnetite, and hematite in the exoskarn. Epidote replaces pyroxene and magnetite in endoskarn and exoskarn zones, respectively.

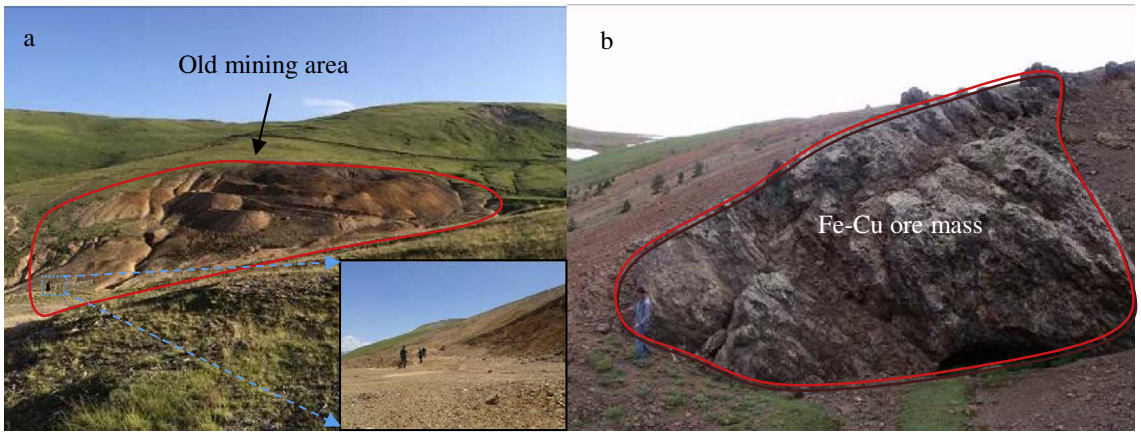

Fig. 7. a) The old mining area and b) ore zone from the Eğrikar Fe-Cu skarn mineralization.

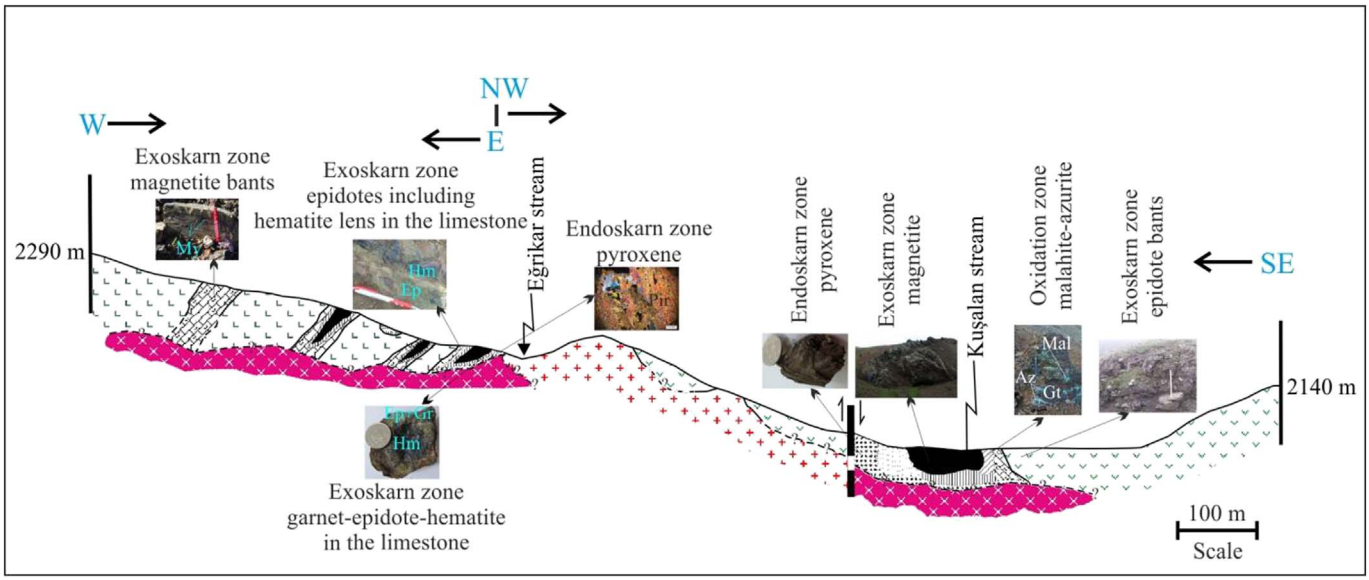

Fig. 8. The cross section of the Eğrikar Fe-Cu skarn mineralization. Symbols are the same as in Fig. 2.

The epidote is Fe-rich with Fe/(Fe + Al) ratios ranging from 0.28 to 0.44 in endoskarn and endo-exoskarn transitional zones and from 0.22 to 0.42 in the exoskarn zone. The Fe/(Fe + Al) ratio of exoskarn epidote from the Eğrikar Fe–Cu skarn is similar to the Fe/(Fe + Al) of epidote in the Ayazmant Fe–Cu skarn (Oyman, 2010) and Kara magnetite–scheelite skarn (Zaw and Singoyi, 2000).

Magnetite is found with epidote and quartz. Some magnetites are replaced with hematite laths. Furthermore, radial and specular hematites are dominant in the exoskarn zone and shown together with garnet. The SiO_2 and TiO_2 contents of magnetite are within 0.04%–2.04% and 0%–0.18%, respectively. *Chalcopyrite* is a small compound and acts as relict among clinopyroxene, magnetite, and

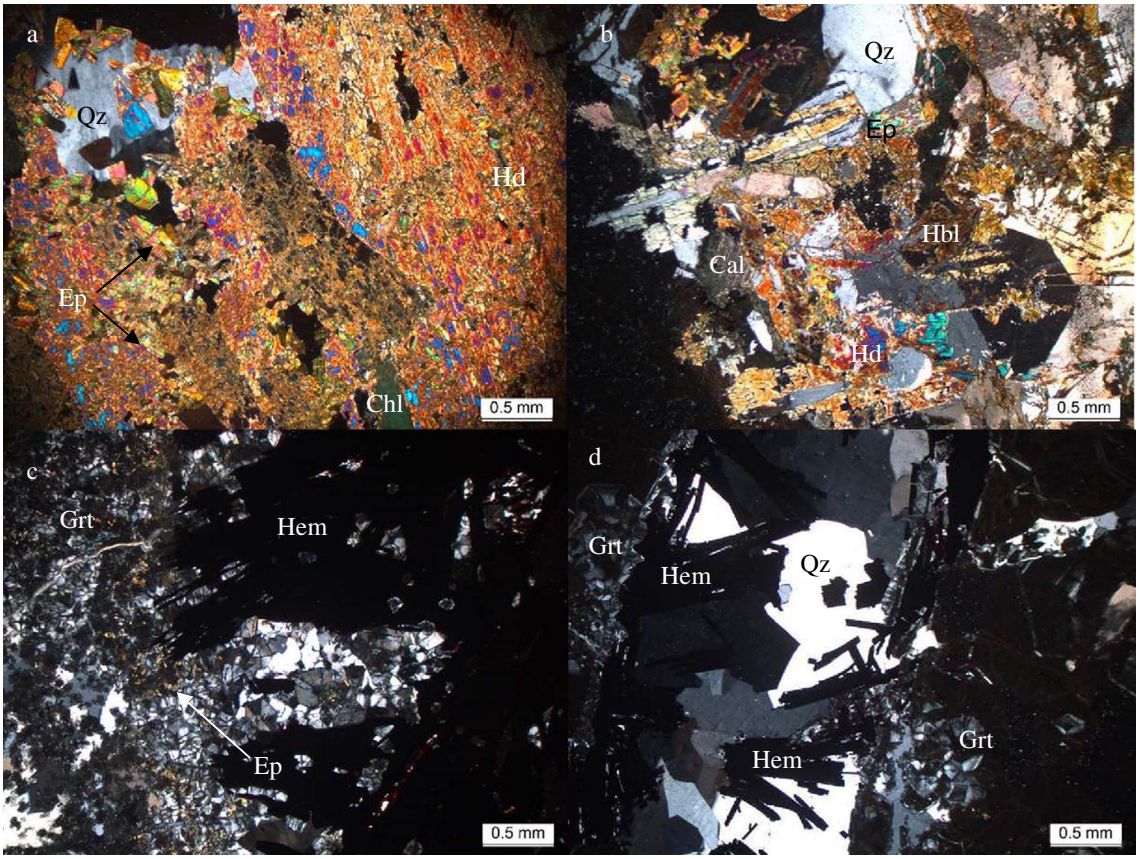

Fig. 9. Microscopic images of skarn minerals. a) the pyroxene replaced by epidote in endoskarn zone (sample number: E48-3, + N), b) pyroxene-hornblende-epidote-quartz-calcite assemblages showing transitional from endoskarn to exoskarn zone (sample number: E48–2, + N), c) garnet-hematite-epidote-quartz in the exoskarn zone (Sample number: E45, + N) and d) hematite and quartz vein between garnets (sample number: E42-10, + N). Hd: Hedenbergite, Grt: Garnet, Hbl: Hornblende, Hem: Hematite, Ep: epidote, Qz: Quartz, Cal: Calcite, Chl: Chlorite.

Table 2
Paragenetic sequence diagram of the Eğrikar (Gümüşhane, Turkey) Fe-Cu skarn mineralization.

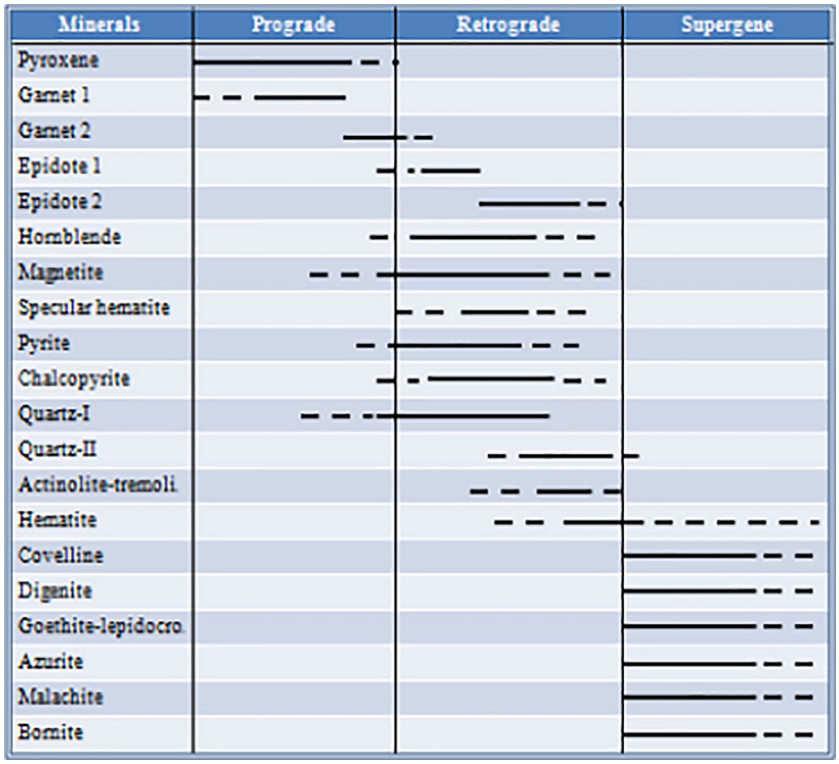

specular hematite. Chalcopyrite is the most common sulfide mineral and partly altered to covellite. The Cu and Fe contents of chalcopyrite change from 34.12% to 35.91% and from 31.27% to 33.73%, respectively, in endoskarn; in exoskarn these contents change from 30.42% to 35.00% and from 30.01% to 33.26%, respectively. *Pyrite* is observed, together with specular hematite, in exoskarn, and it includes less amount of Cu (0%–0.07%) compared to Cu content (0.17%) of the pyrite in the Pena Colorado-Mexico Fe skarn (Zürcher et al., 2001).

4.6. Fluid inclusion

Fluid inclusion analyses were conducted on hedenbergite in endoskarn, and on epidote and quartz in the exoskarn. In the samples from the Eğrikar Fe–Cu skarn area, only primary fluid inclusions yield a reliable homogenization temperatures (Th), first melting temperatures (Tm_{first}), and final ice melting temperatures (Tm_{ice}) measurements (Table 4). Fluid inclusions in hedenbergite, epidote, and quartz are 8–52, 5–13, and 6–19 μm, respectively. The two phases (liquid + vapour) of type I inclusion are identified in hedenbergite, epidote, and quartz, according to the liquid-rich room temperature (Fig. 13). The homogenization temperature for a hedenbergite sample ranges from 350 °C to 380 °C, and the salinity varies from 6.88 wt% to 10.73 wt% NaCl equivalent. For five quartz samples, the homogenization temperature ranges from 316 °C to 395 °C, and the salinity values are between 3.9 wt% and 15.38 wt% NaCl equivalent (Fig. 14). The homogenization temperature of an epidote sample ranges from 365 to 376 °C.

4.7. Stable isotope

In the Eğrikar Fe–Cu skarn mineralization, $\delta^{18}O$, δD, $\delta^{13}C$, and $\delta^{34}S$ values of skarn minerals (hedenbergite, garnet, quartz, magnetite, hedenbergite + amphibole, epidote, calcite, and pyrite) were determined. The results show that skarn minerals were formed from magmatic fluids (Table 5, Fig. 15). Hedenbergite + amphibole, garnet, epidote, and magnetite are close to primary magmatic water, which suggests possible mixing of magmatic and meteoric water. Compared with the C isotope compositions in the other geological environments, the C isotope data of calcite and marble in Eğrikar Fe–Cu skarn are consistent with those of metamorphic and skarns.

The $\delta^{34}S$ values of pyrite in the Eğrikar Fe–Cu skarn mineralization show a considerably narrow range.

5. Discussion

The general characteristics of skarn systems differ among essential ores (W, Cu, Fe, Pb-Zn, Mo, and Sn) (Einaudi et al., 1981). The difference among the skarn mineralization develops as a result of the composition of host rock forming skarn mineralization, fluid composition, skarn formation depth, metamorphism, and metasomatism (Meinert, 1985). The skarn mineralization type is also affected by mineral types in skarn zones, chemical compositions, and formation conditions. In the investigation of mineral compositions from the Eğrikar Fe–Cu skarn mineralization, Si, Al, and Fe immigrate from Erik Granitoid to marble, whereas Ca transfers from marble to Erik Granitoid. Pyroxene type in magnetite-rich skarn displays diopsidic and hedenbergite composition in the presence of magnetite and garnet (Ciobanu and Cook, 2004; Yılmazer, 2012). Endoskarn zone pyroxene from the Eğrikar Fe–Cu skarn mineralization presents a hedenbergite composition; the garnet type in the *endo*- and exoskarn zones is andradite-rich and grossular-rich. In addition, the Mn/Fe values of pyroxene are below 0.15 and close to the values of the Cu-Fe skarn type. The Eğrikar Fe–Cu skarn mineralization contains magnetite and garnet at most. The epidote composition of the Eğrikar Fe–Cu skarn mineralization is pistasitic, which resembles the epidotes of the Fe skarn deposits.

In this study, the SiO_2 content of magnetite in the exoskarn zone

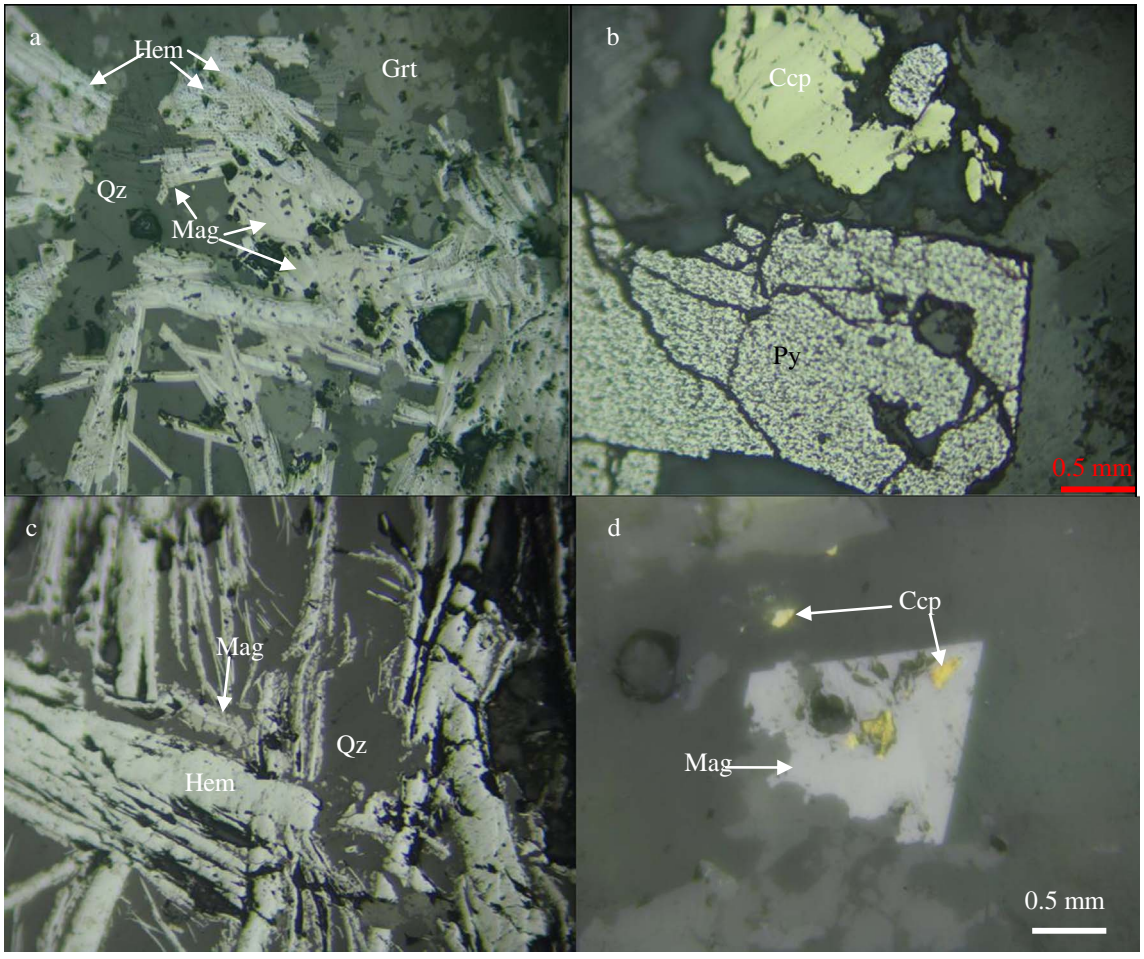

Fig. 10. a) Magnetite replaced by hematite (sample number: E-45), b) cataclastic texture of pyrite (sample number: E-44), c) Hematite laths in magnetite from exoskarn (sample number: E-42-12) and d) magnetite including chalcopyrite (sample number: E-48-3). Mag: magnetite, Hem: hematite, Ccp: chalcopyrite, Py: pyrite, Qz: quartz, Grt: garnet.

is within 0.04%–2.04%. The SiO_2 content increases, whereas the FeO content slightly decreases from the core to the rim. Huberty et al. (2012) determined that silician magnetite has 1%–3% SiO_2 when low-Si magnetite has below 1% SiO_2. Silician magnetite is stabilized relative to magnetite (+ quartz) by more reducing conditions than those for (low-Si) magnetite; the former presence of this organic carbon stabilizes silician magnetite under reducing conditions. Silician and low-Si magnetites in the exoskarn zone from the Eğrikar Fe–Cu skarn mineralization show more reducing (low oxygen fugacity) condition than those of *Si*-free magnetite.

The oxygen isotope values of the low-Si magnetite from the Eğrikar Fe–Cu skarn mineralization range from 1‰ to − 1.6‰. The oxygen isotope (1.3‰ ile 4.6) values of silician magnetite are higher than the oxygen isotope (− 5.6‰ ile 3.8) values of low-Si magnetite (Li et al., 2013). Low-Si magnetite is the earliest magnetite occurrence (Huberty et al., 2012). Low-Si magnetite shows a large variation in $\delta^{18}O$ values, indicating the formation over a wide range of temperature (until 300 °C) or different degrees of isotopic exchange during metamorphism. Magnetite with the lowest $\delta^{18}O$ values represents the most pristine, least exchanged magnetite (Li et al., 2013). In the study area, 255 °C and 438 °C were calculated using the oxygen isotope values of the low-Si magnetite–epidote pair; this finding supported a wide temperature range during metamorphism.

Type I (L + V) fluid inclusion data from Eğrikar Fe–Cu skarn minerals are plotted in "Metamorphic Fluids" field (Fig. 15a). The homogenization temperatures and salinity values are similar to those of Type I inclusions in vesuvianite of the proximal zone from the Susurluk skarn deposit (> 437 °C and mean 11.1% NaCl equivalent, respectively) (Orhan et al., 2010) as well as to those of Type I inclusions of the second phase in vesuvianite and third phase in quartz from Kara magnetite–scheelite skarn mineralization (362 °C–571 °C for vesuvianite and 295.5–359 °C for quartz; and 16.3%–17.8% NaCl equivalent for vesuvianite and 13.4%–15.3% NaCl equivalent for quartz) (Singoyi and Zaw, 2001). These findings indicate magmatic fluids. In addition, low salinity values show a slight dilution by meteoric fluids.

The isotope values of fluids in equilibrium with the magnetite–epidote pair using the temperatures (255 °C and 438 °C) derived from the oxygen isotope values of magnetite-epidote pair were calculated (Table 6). The isotope composition of these fluids falls in "primary magmatic water" field and decreases with decreasing temperature (Fig. 16). Furthermore, the isotope values of fluids in equilibrium with the quartz using the temperatures (255 °C and 438 °C) obtained from fluid inclusion of quartz were calculated and determined to be variable with temperature (Fig. 16). Xu et al. (2015) determined that fluids occurring in prograde skarn were derived from magmatic origin based on $\delta^{18}O_{fluid}$ and δD_{fluid} of fluids being together with garnet, clinopyroxene, quartz, and calcite; these fluids are also affected by meteoric water in retrograde

Table 3
Microchemical analyses of the pyroxene, garnet, epidote, magnetite, chalcopyrite and pyrite from Eğrikar Fe-Cu skarn mineralization.

Mineral	Pyroxene						Garnet 1		Garnet 2			
Zone	Endoskarn						Endo-exoskarn		Exoskarn			
Sample	E43-1		E48-2		E48-3		E48-2		E42-13		E42-1	
Element	Min.	Max.	Min	Max.	Min.	Max.	Min.	Max.	Min.	Max.	Min.	Max.
SiO_2	47.79	52.78	46.12	48.51	48.55	50.46	47.85	49.45	34.95	37.23	35.76	37.21
TiO_2	b.d.l.	0.01	0.02	b.d.l.	0.02	0.02	0.06	0.02	1.13	0.68	0.09	0.26
Al_2O_3	1.18	0.19	1.65	0.10	0.17	0.09	1.26	0.19	5.76	12.06	5.65	5.71
FeO^t	22.52	19.62	22.83	24.96	24.69	20.78	23.58	22.61	20.27	13.41	21.5	20.98
MnO	4.25	5.41	4.96	3.59	3.93	1.76	4.92	5.25	1.32	1.24	1.35	1.26
MgO	2.15	0.65	1.38	0.87	1.03	4.93	1.08	1.26	b.d.l.	0.01	b.d.l.	0.01
CaO	22.27	19.44	22.25	22.40	22.90	23.60	22.46	22.86	33.60	34.55	33.17	32.73
Na_2O	0.43	0.07	0.28	0.17	0.19	0.19						
Total	100.6	98.16	99.49	100.58	101.49	101.84	101.20	101.65	97.04	99.18	97.52	98.16
6 oxygen							12 oxygen					
Si	1.94	2.13	1.89	1.98	1.97	1.98	3.87	3.98	2.89	2.94	2.94	3.04
Ti	–	0.00	0.00	–	0.00	0.00	0.00	0.00	0.07	0.04	0.01	0.02
Al	0.06	0.00	0.08	0.00	0.01	0.00	0.12	0.02	0.56	1.12	0.55	0.55
Fe^{+3}	0.14	0.00	0.17	0.06	0.08	0.06	0.13	0.02	1.41	0.88	1.45	1.26
Fe^{+2}	0.62	0.68	0.61	0.80	0.74	0.60	1.46	1.50	0.00	0.01	0.03	0.18
Mn	0.15	0.19	0.17	0.12	0.13	0.05	0.34	0.36	0.09	0.08	0.09	0.09
Mg	0.13	0.04	0.08	0.05	0.06	0.28	0.13	0.15	–	0.00	–	0.00
Ca	0.97	0.84	0.97	0.98	0.99	0.99	1.95	1.97	2.98	2.92	2.93	2.87
Na	0.03	0.01	0.02	0.01	0.01	0.01	–	–	–	–	–	–
Hd	73.21	75.34	75.31	82.79	80.82	66.15	Ad 0.93	0.99	0.71	0.44	0.73	0.72
Jo	14.20	20.35	16.57	12.06	13.13	5.71	Gr 0.06	0.01	0.28	0.54	0.26	0.27
Di	12.60	4.31	8.12	5.15	6.06	28.14	Sp 0.01	0.00	0.01	0.02	0.01	0.01
Mn/Fe	0.19	0.27	0.21	0.13	0.16	0.08	Al 0.00	0.00	0.00	0.00	0.00	0.00

Ferric Fe is calculated according to Droop (1987).

Mineral	Garnet 2								Epidote 1					
Zone	Exoskarn								Endoskarn		Endo-exoskarn		Exoskarn	
Sample	E42–8		E42–12		E45		E42–10		E48–3		E48–2		E42–8	
Element	Min.	Max.	Min.	Max.	Min.	Max.	Min.	Max.	Min.	Max.	Min.	Max.	Min.	Max.
SiO_2	36.14	37.27	35.03	36.33	33.90	39.38	34.26	36.32	36.42	37.70	37.00	38.40	36.60	37.60
TiO_2	0.01	b.d.l.	0.07	0.03	0.12	0.56	b.d.l.	b.d.l.	0.06	0.08	0.26	0.04	0.10	b.d.l.
Al_2O_3	6.08	6.59	5.93	6.50	6.15	5.20	0.32	6.35	18.28	24.00	18.20	24.20	18.70	20.10
FeO^t	20.93	20.70	20.86	20.22	26.71	21.30	28.70	21.27	19.84	13.10	19.60	13.60	18.50	17.50
MnO	1.34	1.59	1.62	2.64	1.88	1.34	0.53	1.63	0.69	0.52	0.23	0.32	0.14	0.16
MgO	0.02	b.d.l.	0.01	b.d.l.	b.d.l.	b.d.l.	b.d.l.	0.01	b.d.l.	b.d.l.	b.d.l.	b.d.l.	0.02	b.d.l.
CaO	33.39	32.82	32.43	31.64	29.86	30.81	32.69	32.24	22.62	23.40	22.80	23.10	22.80	23.20
Na_2O									0.01	b.d.l.	b.d.l.	0.01	b.d.l.	0.01
H_2O									1.76	1.85	1.77	1.87	1.76	1.80
Total	97.91	98.97	95.94	97.36	98.63	98.59	96.50	97.83	99.69	101.00	99.80	101.00	98.60.	100.00
12 oxygen									25 oxygen					
Si	2.96	3.02	2.93	2.99	2.79	3.22	2.91	2.98	5.97	5.87	6.03	5.92	6.01	6.01
Ti	0.00	–	0.00	0.00	0.01	0.03	–	–	0.01	0.01	0.03	0.00	0.01	–
Al	0.59	0.63	0.58	0.63	0.60	0.50	0.03	0.61	3.53	4.40	3.49	4.40	3.62	3.79
Fe^{3+}	1.40	1.26	1.45	1.30	1.67	0.95	1.95	1.34	2.72	1.71	2.67	1.75		
Fe^{2+}	0.03	0.14	0.01	0.10	0.17	0.50	0.09	0.12	0.09	0.07	0.03	0.04	2.53	2.34
Mn	0.09	0.11	0.11	0.18	0.13	0.09	0.04	0.11	–	–	–	–	0.02	0.02
Mg	0.00	–	0.00	–	–	–	–	0.00	3.97	3.91	3.97	3.81	0.00	–
Ca	2.93	2.85	2.91	2.79	2.63	2.70	2.98	2.83	0.00	–	–	0.00	4.01	3.97
Na									0.96	0.96	0.96	0.96	–	0.00
OH									16.30	16.00	16.20	15.90	0.96	0.96
Ad	0.71	0.69	0.71	0.69	0.75	0.74	0.98	0.70						
Gr	0.28	0.30	0.28	0.29	0.23	0.25	0.02	0.28						
Sp	0.01	0.01	0.01	0.02	0.01	0.01	0.00	0.01						
Al	0.00	0.00	0.00	0.00	0.00	0.00	0.00	0.00						
Py	0.00	0.00	0.00	0.00	0.00	0.00	0.00	0.00						
							Fe/(Fe + Al)		0.44	0.28	0.43	0.28	0.41	0.38

(continued on next page)

Table 3 *(continued)*

Mineral	Epidote 1						Epidote 2					
Zone	Exoskarn						Exoskarn					
Sample	E41		E45		E42–10		E49k		E42–13		E42–12	
Element	Min.	Max.	Min.	Max.	Min.	Max.	Min.	Max.	Min.	Max.	Min.	Max.
SiO_2	37.32	38.24	36.62	38.81	36.34	37.50	36.04	37.74	36.96	38.95	36.18	37.80
TiO_2	0.03	0.02	0.06	0.04	0.04	0.04	b.d.l.	0.04	0.04	0.06	0.04	0.08
Al_2O_3	19.07	21.21	20.57	25.40	18.54	21.27	18.78	21.49	19.66	26.42	19.23	23.70
FeO^t	18.44	15.84	16.96	10.85	18.53	15.84	18.67	15.79	17.43	9.56	17.16	12.50
MnO	0.27	0.59	0.19	0.56	0.09	0.15	0.90	0.33	0.20	0.42	0.32	0.30
MgO	0.06	0.08	b.d.l.	0.25	0.01	0.02	0.01	b.d.l.	b.d.l.	0.06	b.d.l.	b.d.l.
CaO	22.58	22.60	23.27	24.08	22.70	22.74	22.26	23.36	22.55	23.93	22.30	23.10
Na_2O	0.01	b.d.l.	0.01	0.01	b.d.l.	b.d.l.	b.d.l.	b.d.l.	0.02	0.01	0.02	0.01
H_2O	1.78	1.82	1.79	1.90	1.74	1.80	1.75	1.82	1.77	1.90	1.74	1.83
Total	99.56	100.4	99.46	101.90	98.00	99.36	98.41	100.60	98.62	101.30	96.98	99.30
25 oxygen												
Si	6.05	6.04	5.91	5.89	6.01	5.99	5.95	5.97	6.02	5.90	6.00	5.93
Ti	0.00	0.00	0.01	0.01	0.01	0.01	–	0.01	0.00	0.01	0.01	0.01
Al	3.64	3.95	3.91	4.55	3.61	4.01	3.66	4.01	3.77	4.71	3.76	4.39
Fe^{2+}	2.50	2.09	2.29	1.38	2.56	2.12	2.58	2.09	2.37	1.21	2.38	1.64
Mn	0.04	0.08	0.03	0.07	0.01	0.02	0.13	0.04	0.03	0.05	0.05	0.04
Mg	0.01	0.02	–	0.06	0.00	0.01	0.00	–	–	0.01	–	–
Ca	3.92	3.83	4.02	3.92	4.02	3.89	3.94	3.96	3.93	3.88	3.96	3.89
Na	0.00	–	0.00	0.00	–	–	–	–	0.01	0.00	0.01	0.00
OH	0.96	0.96	0.96	0.96	0.96	0.96	0.96	0.96	0.96	0.96	0.96	0.96
Total	16.17	16.02	16.17	15.87	16.22	16.04	16.26	16.07	16.13	15.78	16.16	15.90
Fe/(Fe + Al)	0.41	0.35	0.37	0.23	0.41	0.35	0.38	0.34	0.39	0.20	0.41	0.27

Mineral	Magnetite													
Zone	Endoskarn				Endo-exoskarn		Exoskarn							
Sample	E43-1		E48-3		E48-2		E41		E42-4		E42-13		E45	
Element	Min.	Max.	Min.	Max.	Min.	Max.	Min.	Max.	Min.	Max.	Min.	Max.	Min.	Max.
SiO_2	0.30	2.04	0.73	1.09	0.05	0.59	0.24	1.44	0.06	0.41	0.25	3.84	0.08	2.30
TiO_2	b.d.l.	0.18	b.d.l.	0.03	b.d.l.	0.26	b.d.l.	0.05	b.d.l.	0.11	0.01	0.07	b.d.l.	0.14
Al_2O_3	0.30	1.07	0.01	0.03	0.30	1.23	0.01	0.17	0.03	0.62	0.01	0.62	0.09	0.28
FeO^t	87.22	90.16	91.78	92.57	89.97	91.26	88.40	90.55	88.03	89.80	85.35	89.87	90.68	92.68
MnO	0.02	0.11	0.38	0.52	b.d.l.	0.76	0.04	0.30	b.d.l.	0.30	b.d.l.	0.19	0.04	0.37
MgO	b.d.l.	0.36	b.d.l.	0.01	b.d.l.	0.02	b.d.l.	0.03	b.d.l.	0.03	b.d.l.	0.01	b.d.l.	0.03
CaO	0.02	0.26	0.02	0.09	b.d.l.	0.25	b.d.l.	0.15	b.d.l.	0.05	b.d.l.	0.17	b.d.l.	0.11
Cr_2O_3	b.d.l.	0.01	b.d.l.	0.02	b.d.l.	0.05	b.d.l.	0.03	b.d.l.	0.03	b.d.l.	0.01	b.d.l.	0.03
Total	87.86	94.19	92.92	94.36	90.32	94.42	88.69	92.72	88.13	91.35	85.62	94.78	91.03	95.94
32 oxygen														
Si	0.09	0.56	0.22	0.33	0.02	0.18	0.08	0.45	0.02	0.13	0.08	1.22	0.03	0.70
Ti	–	0.04	–	0.01	–	0.06	–	0.01	–	0.03	0.01	0.02	–	0.03
Al	0.11	0.40	0.00	0.01	0.11	0.40	0.00	0.06	0.01	0.23	0.07	0.23	0.03	0.10
Fe^{2+}	8.04	8.49	8.12	8.22	7.89	8.12	8.01	8.06	8.01	8.03	8.09	9.11	7.98	8.56
Fe^{3+}	14.56	15.62	15.33	15.54	15.21	15.75	15.29	15.70	15.63	15.94	13.54	15.79	15.78	14.56
Mn	0.01	0.04	0.10	0.14	–	0.20	0.01	0.08	–	0.08	–	0.05	0.01	0.10
Mg	–	0.17	–	0.01	–	0.01	–	0.01	–	0.01	–	0.01	–	0.01
Ca	0.01	0.09	0.01	0.03	–	0.08	–	0.05	–	0.01	–	0.06	–	0.04
Cr	–	0.00	–	0.01	–	0.01	–	0.01	–	0.01	–	0.00	–	0.01

Mineral	Magnetite			Chalcopyrite						Pyrite	
Zone	Exoskarn			Endoskarn				Exoskarn		Exoskarn	
Sample	E49k			E43-1		E48-3		E42-6		E42-6	
Element	Min.	Max.	Element	Min.	Max.	Min.	Max.	Min.	Max.	Min.	Max.

(continued on next page)

Table 3 *(continued)*

Mineral	Magnetite			Chalcopyrite						Pyrite	
Zone	Exoskarn			Endoskarn				Exoskarn		Exoskarn	
Sample	E49k			E43-1		E48-3		E42-6		E42-6	
Element	Min.	Max.	Element	Min.	Max.	Min.	Max.	Min.	Max.	Min.	Max.
SiO_2	1.08	5.04	Cu	34.12	35.91	34.19	34.25	33.76	35.00	46.81	47.75
TiO_2	b.d.l.	0.05	Fe	31.27	33.73	31.27	31.44	30.49	31.24	0.03	0.06
Al_2O_3	b.d.l.	1.15	S	34.54	36.61	34.61	34.77	34.58	35.37	53.94	54.54
FeO^t	87.18	95.52	Total	99.93	106.26	100.07	100.46	98.83	101.61	100.781	102.35
MnO	b.d.l.	0.15									
MgO	b.d.l.	0.25	Cu	0.53	0.56	0.53	0.53	0.53	0.55	0.84	0.86
CaO	b.d.l.	0.90	Fe	0.55	0.60	0.55	0.56	0.58	0.56	0.00	0.00
Cr_2O_3	b.d.l.	0.05	S	1.07	1.14	1.07	1.08	1.08	1.10	1.68	1.70
Total	88.26	103.11									
32 oxygen											
Si	0.33	1.50									
Ti	–	0.01									
Al	–	0.40									
Fe^{2+}	8.64	9.12									
Fe^{3+}	12.59	14.60									
Mn	–	0.04									
Mg	–	0.11									
Ca	–	0.29									
Cr	–	0.01									

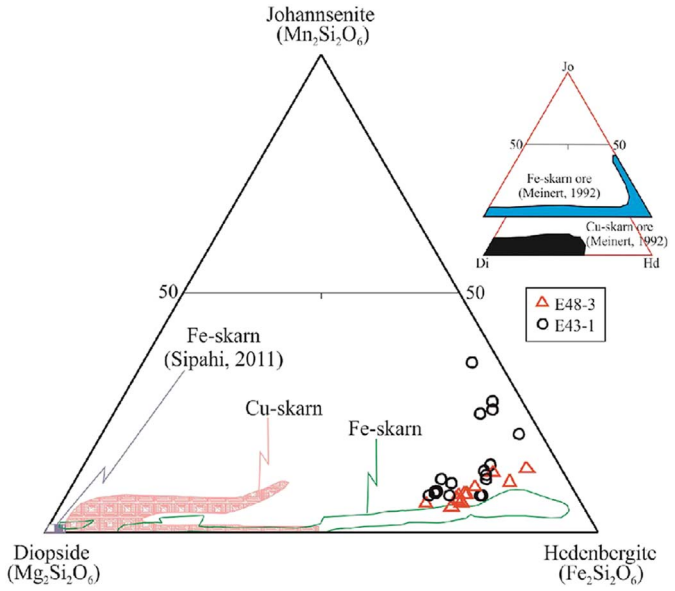

Fig. 11. Classification of clinopyroxene from Eğrikar Fe-Cu skarn mineralization (Cu- and Fe-skarn values from Einaudi and Burt, 1982).

occurrence.

Meteoric water is important in oxygen isotope composition of fluids, depending on temperature decrease at the exoskarn zone in the Eğrikar Fe–Cu skarn mineralization. The $\delta^{18}O$ value of the fluid equilibrium with magnetite and epidote increases according to the isotope composition of the fluid equilibrium with quartz. Therefore, a fluid should be equilibrated with limestone at relatively high temperatures to explain the high values.

The oxygen isotope compositions of magnetite, epidote, and quartz at the exoskarn zone in the Eğrikar Fe–Cu skarn mineralization showed that minerals formed from fluids display an important magmatic composition. The oxygen isotope thermometry calculations of the magnetite and epidote pair at the exoskarn zone determined that these minerals occurred between 255 °C and 438 °C. The magnetite and epidote pair accompany minimal amounts of garnet and quartz in some samples. The temperature for the magnetite–epidote pair was determined as 438 °C, which is marked in Fig. 17 as an early exoskarn phase where garnet is present. The skarn mineral associations in the exoskarn zone of the Eğrikar Fe-Cu skarn mineralization were plotted on magnetite–hematite line at 438 °C. In the garnet-magnetite-epidote-quartz assemblages, garnet is the early phase and replaced with hematite and epidote. Changes in the oxygen fugacity of the quartz accompanied with magnetite were also investigated using temperature (200 °C and 380 °C) values from fluid inclusion studies of the quartz, and stability field experiments of mineral pairs with decreasing temperature (Fig. 17). Fe-rich ore in the Pitkäranta (Russia) polymetallic (Fe, Cu, Sn, and Zn) skarn deposit occurred at low fS_2, low temperatures, and high fO_2 environmental conditions, whereas Cu-rich ore occurred at high fS_2 and high-temperature environment conditions (Valkama et al., 2016). In the Eğrikar Fe–Cu skarn mineralization, pyrite was found, together with magnetite and hematite; The S-isotope values are at a narrow range of $\delta^{34}S$ values, which show a magmatic origin. All of these observations support the sulfur content of ore-forming fluids at the beginning of the skarn formation. In oxidized fluids, a large amount of sulfur can be present as $(SO_4)^{2-}$; consequently, the solubility of Fe is not limited at high temperatures (Jansson and Allen, 2013). Low S content and abundant minerals with ferric Fe show a large amount of oxidized fluids. The Eğrikar Fe–Cu skarn mineralization was formed by Erik Granitoid with medium K calc-alkaline and peraluminous to metaluminous. According to zircon and apatite thermometry, the calculated setting temperature values for Erik Granitoid are between 688 °C and 828 °C (Sipahi et al., 2016). The temperature value of the hedenbergite–garnet pair in the *endo-* and exoskarn zone from the Eğrikar Fe–Cu skarn mineralization was calculated from the mineral chemistry of the hedenbergite–garnet pair according to the methods of Ravna (2000) and estimated at 377 °C–446 °C. The

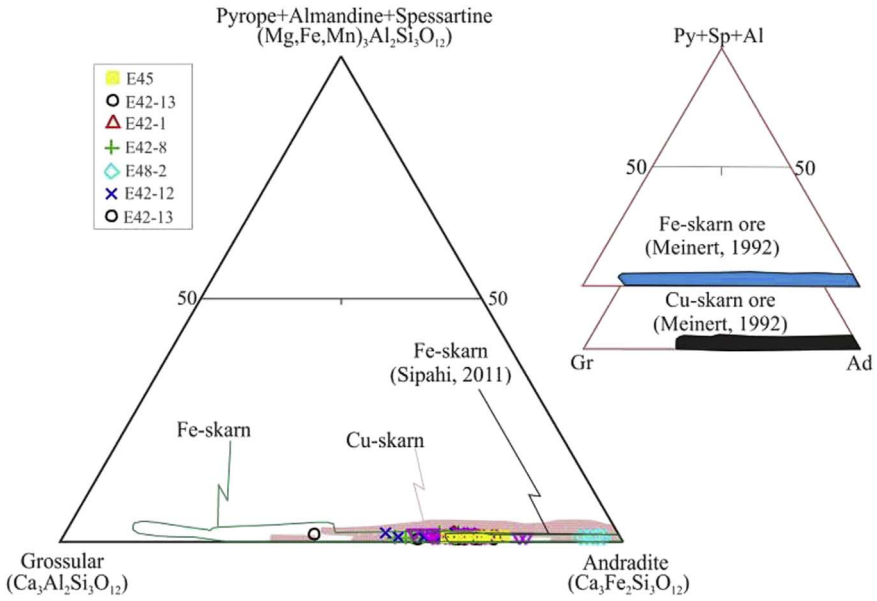

Fig. 12. Ternary diagram showing compositional variations of garnet from the Eğrikar Fe-Cu skarn mineralization.

Table 4
Fluid inclusion analysis results of quartz, epidote, hedenbergite from Eğrikar Fe-Cu skarn mineralization.

Sample number	Host mineral	Inclusion type	Th (°C)	Tm_{first} (°C	Tm_{ice} (°C)	Salinity (wt% NaCl equiv.)
E48-2	Hedenbergite (n = 4)	Type I	350–380	(− 34.2)–(− 52.4)	(− 4.3)–(− 7.2)	6.88–10.73
E38	Quartz	Type I	332–375	(− 19.1)–(− 42.1)	(− 2.3)–(− 7.5)	3.9–11.10
E42-1	Quartz	Type I	199–212	− 28.3	0.2	15.38
E42-7	Epidote	Type I	365–376	–	–	–
E42-7	Quartz	Type I	335–342		(− 3.3)–(− 6.1)	5.41–9.34
E43-3	Quartz	Type I	360–372		(− 2.7)–(− 4.1)	4.5–6.6
E43-4	Quartz	Type I	316–395		(− 2.3)–(− 5.1)	3.9–8

temperature values (255–438 °C) calculated from the oxygen isotope compositions of the magnetite–epidote pair were interpreted with those (200–380 °C) obtained from fluid inclusions of quartz minerals in exoskarn zone from Eğrikar Fe–Cu skarn mineralization with setting temperature values (688–828 °C) of the Erik Granitoid. The results indicated that skarn occurrence started at 750 °C with the settle of the Erik Granitoid. Hedenbergitic diopside-forming temperatures, together with magnetite in Ayazmant Fe–Cu skarn deposit, are between 497 °C and 576 °C (Oyman, 2010). The hedenbergite-forming temperature from fluid inclusion of the hedenbergite, which accompanies minimal amounts of magnetite and quartz in endoskarn zone, is 350 °C–500 °C (Sipahi et al., 2016).

Carbon and oxygen isotope compositions of limestone and calcite minerals reflect the effect of the fluid-rock, and indicate the effect of temperature in mineral formation (Zheng and Hoefs, 1993). Carbon and oxygen isotope values of limestone and calcite minerals in the Eğrikar Fe–Cu skarn mineralization fall in retrograde alteration field (Fig. 18). Carbon and oxygen isotope values of limestone and calcite minerals reflect variation in temperature. In addition, oxygen isotope compositions of samples are present in a narrow range, which implies the effect of calcite-forming similar fluids.

The sulfur isotope characteristics of pyrite from Eğrikar Fe–Cu skarn mineralization suggested a single well-homogenized source of sulfur and magmatic origins; they are also similar to the S-isotope values of sulfides in Edong (China) Cu-Fe skarn deposit (Xie et al., 2015), pyrite in Baijiazi (China) Zn-Pb skarn deposit (Zhao et al., 2003), pyrite in Şamlı (Balıkesir, Turkey) Fe-oxide Cu skarn deposit (Yılmazer et al., 2014), and arsenopyrite in Salanfe (France) W-Au-As skarn deposit (Chiarada, 2003); however, they are different from the S-isotope compositions of pyrites in Ayazmant (Balıkesir, Turkey) Fe–Cu skarn (Oyman, 2010) and Eğrigöz (Kütahya, Turkey) Fe skarn deposit and sulpides in Kotana (Giresun, Turkey) Fe skarn (Çiftçi, 2011) (Fig. 19). This difference is due to the occurrence of pyrites in Ayazmant Fe–Cu skarn deposit and Eğrigöz Fe skarn deposit in the late phase; by contrast, pyrites, analyzed in Eğrikar Fe–Cu skarn mineralization, forms in the retrograde stage.

6. Conclusions

1. Erik Granitoid with an age of 42.3 ± 1.0 Ma for U–Pb zircon geochronology is medium K calc-alkaline and peraluminous to metaluminous, and suggests a magmatic arc-related environment based on their trace element concentrations. The geochemistry of Erik granitoid is close to that of pluton association with Fe- and Cu-skarn deposits. In addition, Erik Granitoid is emplaced into the Upper Cretaceous sandy carbonates hosting Eğrikar Fe–Cu skarn mineralization.
2. In the Eğrikar Fe–Cu skarn mineralization, hedenbergitic ($Di_{4.31–28.14}Hd_{59.29–80.82}Jo_{5.0–35.55}$) clinopyroxene with less diopside and johannsenite is observed in the endoskarn zone. Hedenbergite has low Mn/Fe ratios (< 0.15) and exhibits poor TiO_2. The Mn/Fe

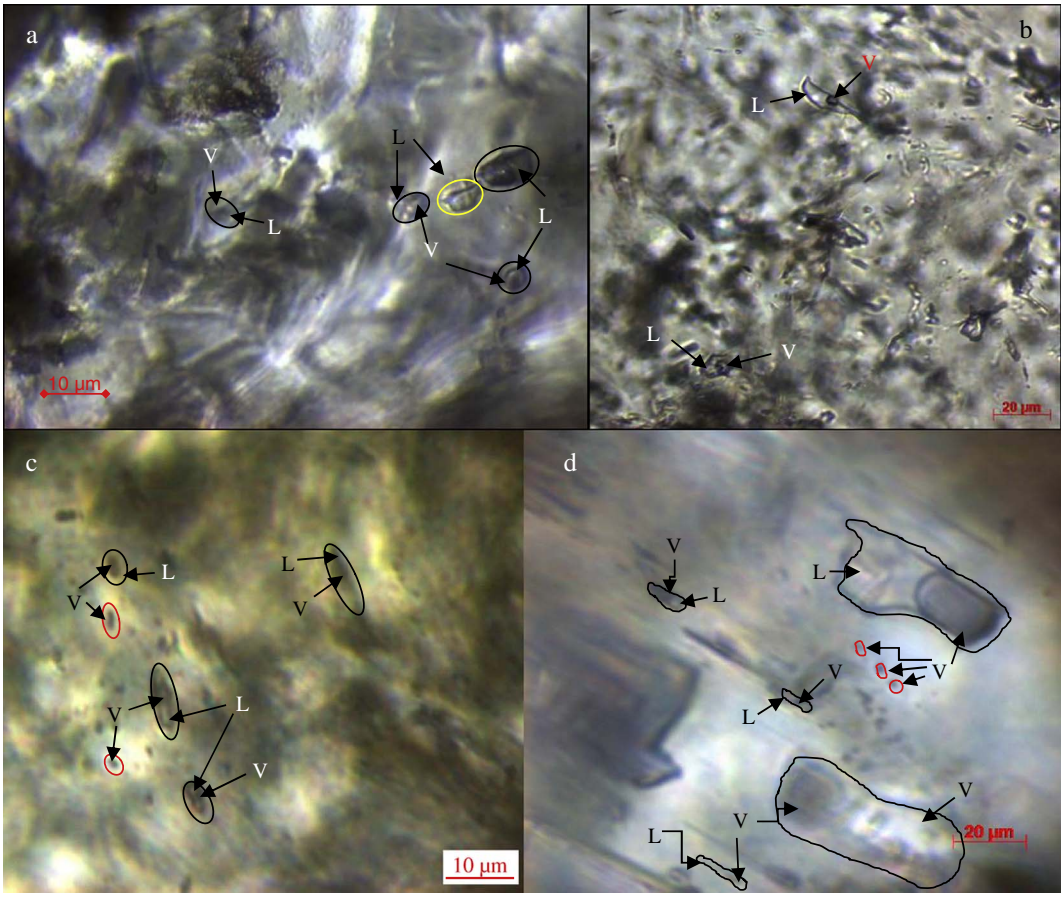

Fig. 13. Photomicrographs of primary fluid inclusions at room temperature in hedenbergite, epidote and quartz from Eğrikar Fe-Cu skarn deposit. a) Type I two phases (liquid + vapour) and liquid-rich and single (liquid) phase from exoskarn zone quartz (sample number: E38), b) type I two phases (liquid + vapour) from exoskarn zone quartz (sample number: E42-1), c) Type I two phases (liquid + vapour) and liquid-rich and single (vapour) phase from exoskarn zone epidote (sample number: E42-1) and d) type I two phases (liquid + vapour) and liquid-rich and single (vapour) phase from *endo*-exoskarn zone hedenbergite (sample number: E48-2). L: liquid, V: vapour.

values of pyroxene from Eğrikar Fe–Cu skarn mineralization are similar to the Cu-Fe skarn-type deposit.

3. The garnet type in the *endo*-exoskarn transitional zone from Eğrikar Fe–Cu skarn mineralization is represented by andradite ($Ad_{91-99}Gr_{01-07}$) with a narrow range of variation in composition and grossular-andradite ($Ad_{44-95}Gr_{05-54}$) in the exoskarn zone. The Ad/Gr ratio of garnet increases in exoskarn zone from Eğrikar Fe–Cu skarn mineralization, and the $f(O_2)$ also increases.
4. Epidote ($Ca_{3.86-4.04}Fe_{1.64-2.67}Al_{3.47-4.77}Si_{5.82-6.02}O_{24}(OH)_{0.96-1.00}$) from Eğrikar Fe–Cu skarn mineralization has high Fe/(Fe + Al) ratio (mean, 0.34), which is typical for Fe-skarn deposits.
5. Magnetite from Eğrikar Fe–Cu skarn mineralization has both low-Si and silician in exoskarn zone. SiO_2 content of hematite increases from core to rim, whereas its FeO content decreases from core to rim. Silician and low-Si magnetite in the exoskarn from the Eğrikar Fe–Cu skarn mineralization form in further reducing (low oxygen fugacity) conditions according to magnetite.
6. The primary fluid inclusion studies of Type I in hedenbergite, epidote, and quartz from Eğrikar Fe–Cu skarn mineralization provide a wide homogenization temperature range of 200–500 °C and a wide salinity range of 3.9–15.38 equiv. wt% NaCl for endo-exoskarn zone. The homogenization temperature and salinity values suggest the effect of cooling with isothermal mixing of relatively two different fluids in mineral precipitation. The homogenization temperature and density (0.75–0.60 g/cm^3) of fluid inclusion in skarn minerals support the skarn origin. The first melting values in hedenbergite and quartz range from 34.2 °C to −52.4 °C and −28.3 °C to −38.5 °C, respectively, and proposed the NaCl + $CaCl_2$ ± $FeCl_2$ + H_2O-composition fluids in the system.
7. The oxygen isotope compositions of hedenbergite, hedenbergite + amphibole, garnet, epidote, magnetite, quartz, and calcite in the Eğrikar Fe–Cu skarn mineralization vary in a narrow range and indicate playing a role similar property fluids in mineral formation. In addition, the δD values of hydrous minerals and fluid composition in equilibrium with magnetite–epidote pair support the magmatic origin and show a little mixing from meteoric source, depending on a decrease of temperature.
8. Sulfur isotope values of pyrites vary in a narrow range and show a magmatic origin. This indicates that ore-forming fluids include sulfur at the beginning of the skarn formation and occur in low fS and high fO_2 environment conditions.

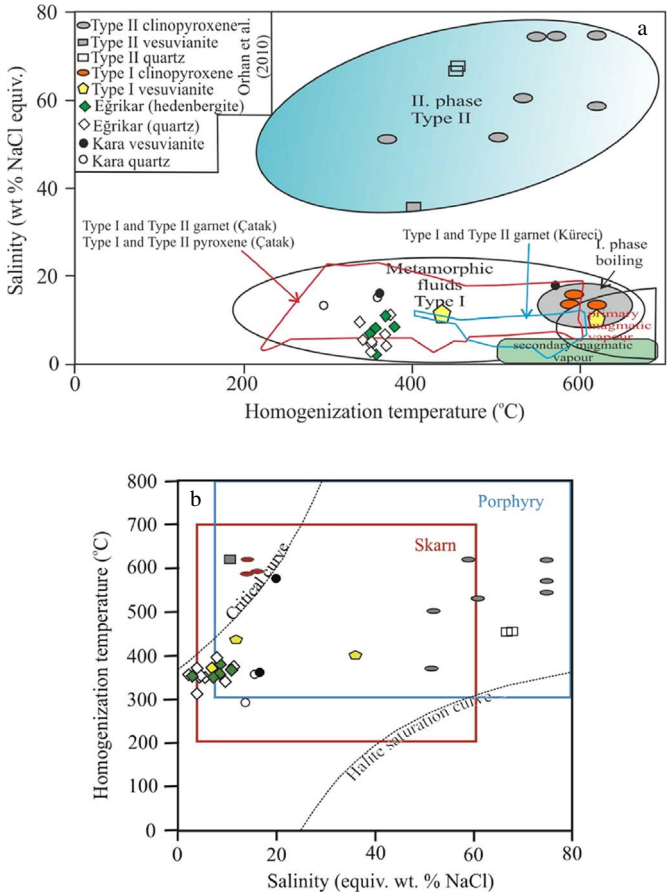

Fig. 14. a) Homogenization temperatures (°C) against salinity (wt% NaCl equiv.) values (various solutions are from Bodnar, 1999; Çatak and Küreci data from Oyman et al., 2013) and b) Salinity (wt% NaCl equiv.) against homogenization temperatures (°C) values (Wilkinson, 2001) of fluid inclusions of samples in the Eğrikar Fe-Cu skarn mineralization.

Table 5
Isotope compositions of skarn minerals and rocks.

Sample number	Mineral and rock name	δD_{VMSOW} ‰	$\delta^{18}O_{VSMOW}$ ‰	$\delta^{13}C_{VPDB}$ ‰	$\delta^{34}S_{VPDB}$ ‰	Skarn zone
E48	Hedenbergite		4.1			Endoskarn
E48-2	Hedenbergite + amphibole	− 96	4.7			Endo-exoskarn
E48-3A	Hedenbergite + amphibole	− 104	4.1			
E12	Quartz		15.2			Exoskarn
E38	Quartz		8.5			
E43	Quartz		10.1			
E42	Magnetite		1.0			
	Epidote	− 73	7.9			
E42-3	Magnetite (Hematite)		− 1.6			
	Epidote	− 55	9.2			
E42-10	Garnet		3.4			
	Magnetite		4.4			
E44	Pyrite				4.4	
E21	Pyrite				3.0	
E1	Hematite		− 2.9			
E11k	Calcite		9.6	− 3.2		
E29	Marble		9.2	2.8		
E126	Crystallized limestone		11.1	1.6		
E45a	Crystallized limestone		9.1	1.6		
E6c	Limestone		8.7	1.2		
E52b	Sandy limestone		9.1	2.5		
E54	Eğrikar Monzogranite		8.9			
K16	Erik Granitoide		6.6			

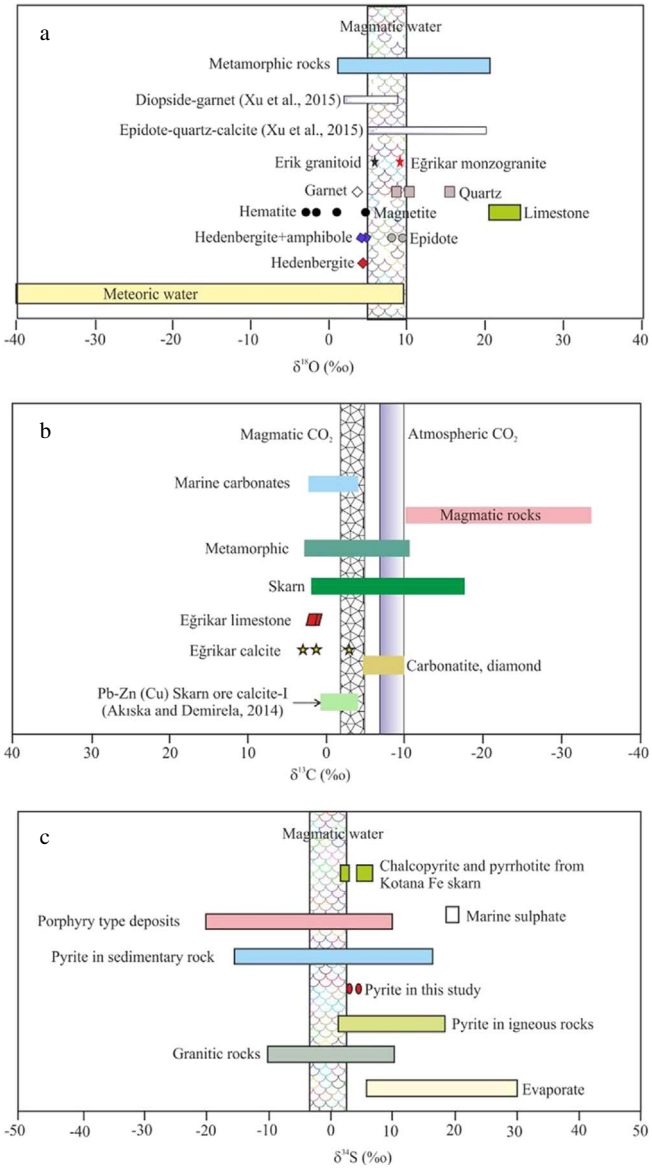

Fig. 15. a) $\delta^{18}O$ (‰) isotope variations of the hedenbergite, garnet, magnetite, hedenbergite + amphibole, epidote and quartz minerals (other data from Hoefs, 1987), b) $\delta^{18}C$ (‰) isotope changings of the limestone and calcite minerals (other data from Hoefs, 1987) and c) $\delta^{18}S$ (‰) changing of the pyrite (data of various rocks, geological environments and ore types from Ohmoto and Rye, 1979; Field and Fifarek, 1985; Hoefs, 1987) from Eğrikar Fe-Cu skarn mineralization.

Table 6
The $\delta^{18}O$ and δD isotope compositions of fuid inclusions in equilibrium with minerals of the exoskarn zone from the Eğrikar Fe-Cu skarn mineralization.

Sample	$\delta^{18}O_{mineral}$ (‰) VSMOW			$\delta D_{mineral}$ (‰) VMSOW	Calculated $\delta^{18}O_{fluid}$ (‰)		T °C
	Magnetite	Quartz	Epidote	Epidote	Quartz-water	Magnetite-epidote	
E12	–	15.2	–	–	2.99–7.43[a]		200–290[b]
E38	–	8.5	–	–	1.20–3.47[a]		245–380[b]
E42	1.0	–	7.9	− 73		8.59[c]	438[c]
E42-3	− 1.6 (with hematite)	–	9.2	− 55		7.17[c]	255[c]

[a] Friedman and O'Neil (1977).
[b] Fluid inclusion.
[c] Zheng and Simon (1991); Zheng (1993).

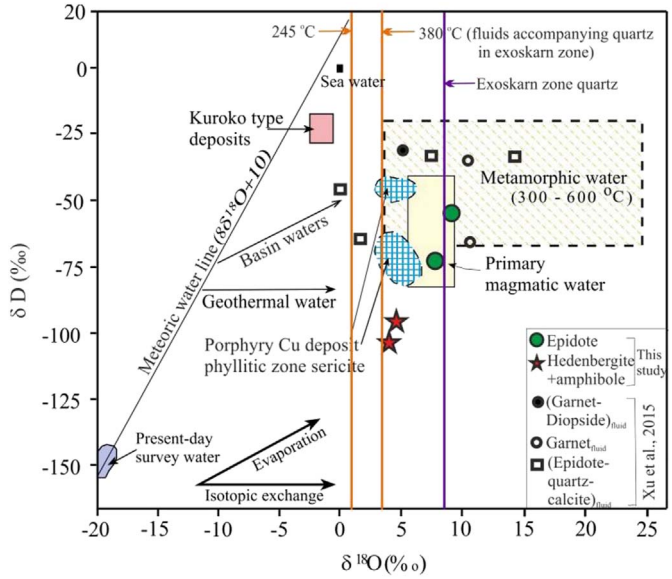

Fig. 16. $\delta^{18}O$ vs δD composition variations of skarn minerals and fluids accompanying skarn minerals in Eğrikar Fe-Cu skarn mineralization (modified from Hoefs, 1987).

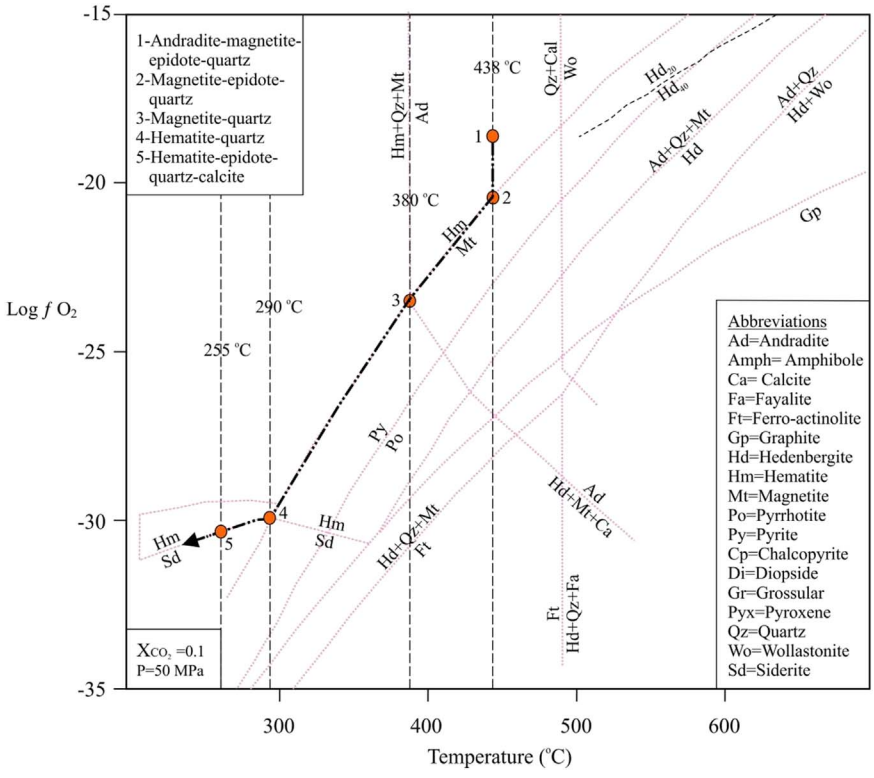

Fig. 17. Temperature vs. *f*O2 diagram showing the stability fields of skarn minerals from exoskarn zone in Eğrikar Fe-Cu skarn mineralization (stability fields of silicate, oxide, sulfur and carbonate minerals from Einaudi et al., 1981; Meinert, 1998). Typical skarn associations were plotted on the basis of magnetite-hematite line.

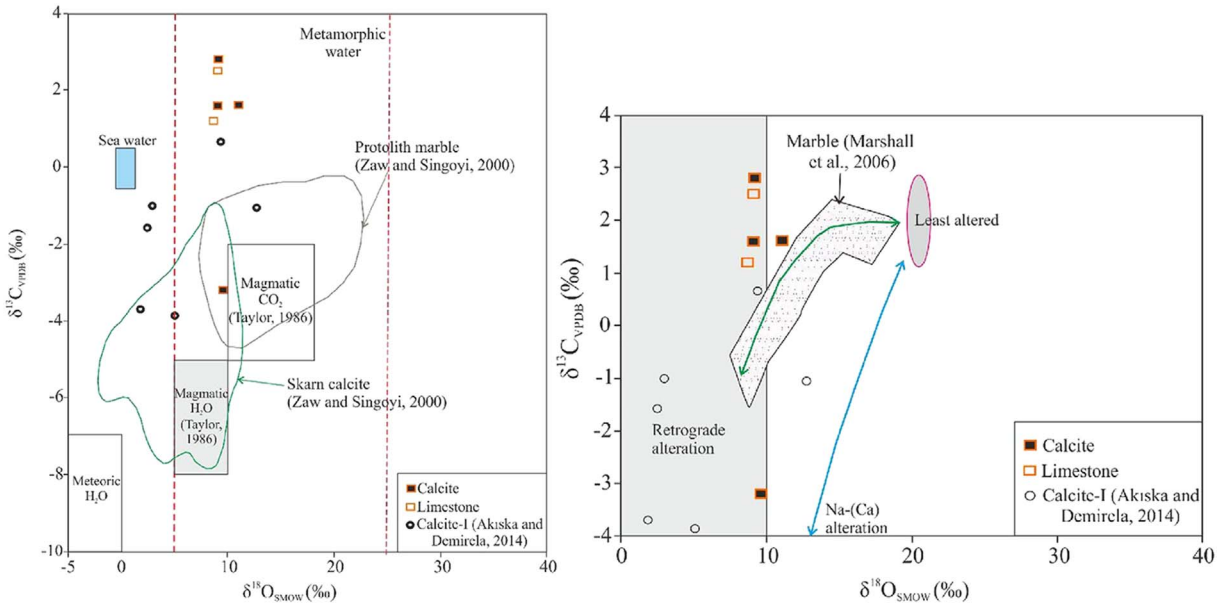

Fig. 18. Plot of $\delta^{13}O_{VPDB}$ and $\delta^{13}O_{SMOW}$ values of the calcite and limestone in the Eğrikar Fe-Cu skarn mineralization (modified from Marshall et al., 2006). Magmatic H_2O field from Taylor (1986) and calcite-I values from Akıska and Demirela (2014)

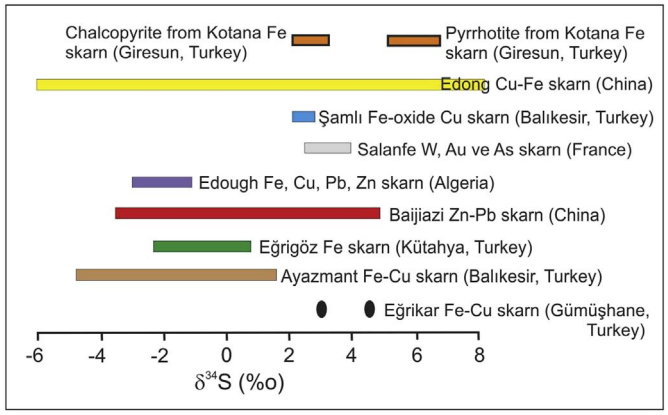

Fig. 19. $\delta^{34}S$ isotope compositions of pyrites in Eğrikar Fe-Cu skarn mineralization are compared to other Fe-Cu deposits. (data in Şamlı Fe-oxide Cu skarn deposit from Yılmazer et al., 2014; Edough Fe-Cu-Pb-Zn skarn deposit from Laouar et al., 2002; Salanfe W-Au-As skarn deposit from Chiarada, 2003; Baijiazi Zn-Pb skarn deposit from Zhao et al., 2003; Ayazmant Fe-Cu skarn deposit from Oyman, 2010; Kotana Fe skarn Deposit from Çiftçi, 2011; Eğrigöz Fe skarn deposit from Oyman et al., 2013).

Acknowledgements

This research was supported by the 114Y013 numbered Turkish Science Foundation (TÜBİTAK). Authors thank to Meral Kaya for the paleontologic analysis and are grateful to handling associate editor Dmitry Konopelko and to anonymous reviewers for their constructive comments to improve the paper. Enes Türk and Tanju Aydurmuş are thanked for their help during the fieldwork.

References

Abu El-Enen, M.M., Okrusch, M., Will, T.M., 2004. Contact metamorphism and metasomatism at a dolerite-limestone contact in the Gebel Yelleq area, Northern Sinai, Egypt. Mineral. Petrol. 81, 135–164.
Akaryalı, E., 2016. Geochemical, fluid inclusion and isotopic (O, H and S) constraints on the origin of Pb–Zn ± Au vein-type mineralizations in the Eastern Pontides Orogenic Belt (NE Turkey). Ore Geol. Rev. 74, 1–14.
Akaryalı, E., Akbulut, K., 2016. Constraints of C–O–S isotope compositions and the origin of the Ünlüpınar volcanic-hosted epithermal Pb–Zn ± Au deposit, Gümüşhane, NE Turkey. J. Asian Earth Sci. 117, 119–134.
Akıska, S., Demirela, G., 2014. Origin of the fluids in the Handeresi, Bağırkaçdere, and Fırıncıkdere (Kalkım, Yenice-Çanakkale) Pb-Zn ± Cu distal skarn deposits. Yerbilimleri 35 (3), 199–218.
Altherr, R., Topuz, G., Siebel, W., Şen, C., Meyer, H.P., Satır, M., 2008. Geochemical and Sr–Nd–Pb isotopic characteristics of Paleocene plagioleucitites from the Eastern Pontides (NE Turkey). Lithos 105, 149–161.
Andersen, T., 2002. Correction of common lead in U-Pb analyses that do not report ^{204}Pb. Chem. Geol. 192, 59–79.
Arslan, M., Aslan, Z., 2006. Mineralogy, petrography and whole-rock geochemistry of the tertiary granitic intrusions in the Eastern Pontides, Turkey. J. Asian Earth Sci. 27, 177–193.
Arslan, M., Tüysüz, N., Korkmaz, S., Kurt, H., 1997. Geochemistry and petrogenesis of the Eastern Pontide volcanic rocks, Northeast Turkey. Chem. Erde 57, 157–187.
Aslaner, M., Van, A., Yalçınalp, B., 1995. General features of the Pontide metallogenic belt. In: Erler, A., Ercan, T., Bingöl, E., Örçen, S. (Eds.), Geology of the Black Sea Region. General Directorate of Mineral Research and Exploration and Chamber of Geological Engineers, Ankara, Turkey, pp. 209–213.
Barton, M.D., Ilchik, R.P., Marikos, M.A., 1990. Metasomatism, in Kerrick, D.M., ed., contact metamorphism. Rev. Mineral. 26, 321–350.
Black, L.P., Kamo, S.L., Allen, C.M., Aleinikoff, J.N., Davis, D.W., Korsch, R.J., Foudoulis, C., 2003. TEMORA 1: a new zircon standard for Phanerozoic U–Pb geochronology. Chem. Geol. 200, 155–170.
Bodnar, R.J., 1999. Hydrothermal solutions. In: Marshall, C.P., Fairbridge, R.W. (Eds.), Encyclopedia of Geochemistry. Kluwer Academic Publishers, Lancaster, pp. 333–337.
Boztuğ, D., Jonckheere, R., Wagner, G.A., Yegingil, Z., 2004. Slow Senonian and fast Palaeocene–Early Eocene uplift of the granitoids in the Central Eastern Pontides, Turkey: apatite fission-track results. Tectonophysics 382, 213–228.
Çamur, M.Z., Güven, İ.H., Er, M., 1996. Geochemical characteristics of the Eastern Pontide volcanics: an example of multiple volcanic cycles in arc evolution. Turk. J. Earth Sci. 5, 123–144.
Çekiç, Y., Güç, A.R., Eroğlu, C.İ., Türkmen, İ., Çağlar, O., Akıncı, S., Kurtoğlu, T., 1985. Giresun G41-C1-C2-C3-C4-D1-D2-D3-D4 Paftalarının Polimetalik Masif Sülfit Cevheri Prospeksiyonu Raporu. In: MTA Raporu, No: 84-8e.
Chiarada, M., 2003. Formation and evolution processes of the Salanfe W-Au-As-skarns (Aiguilles Rouges Masif, western Swiss Alps). Mineral. Deposita 38, 154–168.
Çiftçi, E., 2011. Sphalerite associated with pyrrhotite-chalcopyrite ore occurring in the Kotana Fe-skarn deposit (Giresun, NE Turkey): Exsolution or replacement. Turk. J. Earth Sci. 20, 307–320.
Ciobanu, C.L., Cook, N.J., 2004. Skarn textures and a case study: the Ocna de Fier–Dognecea orefield, Banat, Romania. Ore Geol. Rev. 24, 315–370.
Dokuz, A., Karsli, O., Chen, B., Uysal, I., 2010. Sources and petrogenesis of Jurassic granitoids in the Yusufeli area, Northeastern Turkey: implications for pre- and post-collisional lithospheric thinning of the Eastern Pontides. Tectonophysics 480, 259–279.
Droop, G.T.R., 1987. A general equation for estimating Fe^{+3} concentrations in ferromagnesian silicates and oksides from microprobe analyses, using stoichiometric criteria. Mineral. Mag. 51, 431–435.
Einaudi, M.T., 1982. Descriptions of skarn associated with porphyry copper plutons, Southwestern North America. In: Titley, S.R. (Ed.), Advances in Geology of the Porphyry Copper Deposists, Southwestern North America. Tucson, University of Arizona, pp. 185–210.
Einaudi, M.T., Burt, D.M., 1982. Introduction-terminology, classification and compositionof skarn deposits, a special issue devoted to skarn deposits. Econ. Geol. 77, 745–754.

Einaudi, M.T., Meinert, L.D., Newberry, R.J., 1981. Skarn Deposits. Econ. Geol. 75, 317–391.
Er, M., Serdar, A.M., 1992. Doğu Karadeniz Bölgesinde 1967–1991 yılları arasında yapılan çalışmalar – elde edilen sonuçlar ve yeni maden arama proje önerileri. In: MTA Raporu, (272 p).
Eyüboğlu, Y., Chung, S.L., Santosh, M., Dudas, F.O., Akaryalı, E., 2011. Transition from shoshonitic to adakitic magmatism in the Eastern Pontides, NE Turkey: Implications for slab window melting. Gondwana Res. 19, 413–429.
Field, C.W., Fifarek, R.H., 1985. Light isotope systematics in the epithermal environment. In: Berger, B.R., Bekte, P.M. (Eds.), Geology and Geochemistry of Geothermal Systems. Reviews in Economic Geology, vol. 2. pp. 99–128.
Friedman, I., O'Neil, J.R., 1977. Compilation of stable isotope fractination factors of geochemical interest, in geology and geochemistry of epithermal systems. In: Field, C.W., Fifarek, R.H. (Eds.), Light Stable-isotope Systematics in the Epithermal Environment. Reviews in Economic Geology, vol. 2. pp. 99–128.
Gedikoğlu, A., 1979. Geochronologic etude of Harşit (Giresun–Doğankent) granite complex. In: Turkey Geology Scientific and Technic Diet Abstract Book. 33. pp. 59–60.
Güven, İ.H., 1993. Doğu Pontidler'in 1/250.000 Ölçekli Kompilasyonu, MTA Gen. Müd., Ankara.
Hoefs, J., 1987. Stable Isotope Geochemistry, 3rd ed. Springer, Berlin-Heidelberg-New York (241 p).
Huberty, J.M., Konishi, H., Heck, P.R., Fournelle, J.H., Valley, J.W., Xu, H., 2012. Silician magnetite from the Dales Gorge Member of the Brockman Iron Formation, Hamersley Group, Western Australia. Am. Mineral. 97, 26–37.
İstanbullu, E., 2013. Balıkesir-Dursunbey Skarn Yataklarının Jeolojik, Mineralojik ve Jeokimyasal Özellikleri. Unpublished M.Sc. thesis Fen Bilimleri Enstitüsü, İstanbul Technical University.
Jansson, N.F., Allen, R.L., 2013. Timing and setting of skarn and iron oxide formation at the Smältarmossen calcic iron skarn deposit, Bergslagen, Sweden. Mineral. Deposita 48, 313–339.
Laouar, R., Boyce, A.J., Ahmed-Said, Y., Ouabadi, A., Fallick, A.E., Toubal, A., 2002. Stable isotope study of the igneous, metamorphic and mineralized rocks of the Edough complex, Annaba, Northeast Algeria. J. Afr. Earth Sci. 35, 271–283.
Le Maitre, R.W., Bateman, P., Dudek, A., Keller, J., Lameyre, J., Le Bas, M.J., Sabine, P.A., Schmid, R., Sorensen, H., Streckeisen, A., Wooley, A.R., Zanettin, B.A., 1989. Classification of Igneous Rocks and Glossary of Terms. Blackwell, Oxford.
Leitch, C.H.B., Lentz, D.R., 1994. The Gresens approach to mass balance constraints of alteration systems: methods, pitfalls, examples. In: Lenz, D.R. (Ed.), Alteration and Alteration Processes Associated with ore-Forming Systems. Geological Association of Canada, Short Course Notes Vol. 11. pp. 161–192.
Lentz, D.R., Suzuki, K., 2000. A low F pegmatite-related Mo skarn from the southwestern Grenville Province, Ontario, Canada: phase equilibria and petrogenetic implications. Econ. Geol. 95, 1319–1338.
Li, W., Huberty, J.M., Beard, B.L., Kita, N.T., Valley, J.W., Johnson, C.M., 2013. Contrasting behavior of oxygen and iron isotopes in banded ironformations revealed by in situ isotopic analysis. Earth Planet. Sci. Lett. 384, 132–143.
Ludwig, K.R., 2003. User's manual for Isoplot 3.0: a eochronological toolkit for Microsoft excel. In: Berkeley Geochronology Center, Special Publication. 4. pp. 1–71.
Marshall, L.J., Oliver, N.H.S., Davidson, G.J., 2006. Carbon and oxygen isotope constraints on fluid sources and fluid–wallrock interaction in regional alteration and iron-oxide–copper–gold mineralisation, Eastern Mt Isa Block, Australia. Mineral. Deposita 41, 429–452.
Matsueda, H., 1981. Pyrometasomatic iron-copper ore deposits of the Sampo Mine, Okayama Prefecture, Japan. Part II. The mode of occurrences, mineral paragenesis and chemical compositions of skarn and ore. Akita Univ. Min. Coll. J. 6, 1–43.
Meinert, L.D., 1985. Compositional variation of igneous rocks associated with skarn deposits-chemical evidence for a genetic connection between petrogenesis and mineralization. In: Mineralogical Association of Canada Short Course Series. 23. pp. 401–418.
Meinert, L.D., 1992. Skarn and skarn deposits. Geosci. Can. 19, 145–162.
Meinert, L.D., 1995. Igneous petrogenesis and skarn deposits. Geol. Assoc. Can. Spec. Pap. 40, 569–593.
Meinert, L.D., 1997. Application of skarn deposit zonation models to mineral exploration. Explor. Min. Geol. 6, 185–208.
Meinert, L.D., 1998. A review of skarns that contain gold. In: Lentz, D.R. (Ed.), Mineralized Intrusion-Related Skarn System. Mineralogical Association of Canada Short Course Series Vol. 26. pp. 359–414.
Meinert, L.D., Dipple, G.M., Nicolescu, S., 2005. World skarn deposits. In: Economic Geology. 100th Anniversary Volume. pp. 299–336.
Middlemost, E.A.K., 1994. Naming materials in the magma/igneous rock system. Earth Sci. Rev. 37, 215–224.
Moore, W.J., Mckee, E.H., Akıncı, Ö., 1980. Chemistry and chronology of plutonic rocks in the Pontid mountains, Northern Turkey. In: Symposium of European Copper Deposits, Belgrade, pp. 209–216.
MTA, 2002. 1/500.000 scaled Turkey geology map Trabzon paftası In: Akdeniz, N., Güven, İ. (Eds.), General Directorate of Mineral Research and Exploration (MTA) Publication, (in Turkish).
Murakami, H., 2005. How to Study Skarn Type Deposits, a Short Term Expert Seminar, Submitted to: Remote Sensing Center. MTA. http://staff.aist.go.jp/hmurakami/skarn.pdf (11 p).
Nakano, T., 1998. Pyroxene geochemistry as an indicator for skarn metallogenesis in Japan. In: Lentz, D.R. (Ed.), Mineralized Intrusion-related Skarn Systems. Mineralogical Association of Canada Short Course Series Vol. 26. pp. 147–167.
Nakano, T., Yoshino, T., Shimazaki, H., Shimizu, M., 1994. Pyroxene composition as an indicator in the classification of skarn deposits. Econ. Geol. 89, 1567–1580.
Ohmoto, H., Rye, R.O., 1979. Isotopes sulfur and carbon. In: Barnes, H.L. (Ed.), Geochemistry of Hydrothermal Ore Deposits, Second Edition. John Wiley and Sons Inc., New York, pp. 509–567.
Okay, A.İ., Şahintürk, Ö., 1997. Geology of the Eastern Pontides. In: Robinson, A.G. (Ed.), Regional and Petroleum Geology of the Black Sea and Surrounding Region. Am Assoc Petrol Geol Mem Vol. 68. pp. 291–310.
Okay, A.I., Tüysüz, O., 1999. Tethyan sutures of northern Turkey. In: Durand, B., Jolivet, L., Horváth, F., Séranne, M. (Eds.), The Mediterranean Basins: Tertiary Extension within the Alpine Orogen. Special Publications, Geological Society London Vol. 156. pp. 475–515.
Okay, A.I., Şahintürk, Ö., Yakar, H., 1997. Stratigraphy and tectonics of the Pulur (Bayburt) region in the Eastern Pontides. Miner. Res. Explor. Bull. 119, 1–24.
Orhan, A., Mutlu, H., Hanilçi, N., 2010. Susurluk (Balıkesir) "Oksidan Tip" W-skarnının mikrotermometrik özellikleri. MTA Dergisi 141, 55–71.
Oyman, T., 2010. Geochemistry, mineralogy and genesis of the Ayazmant Fe–Cu skarn deposit in Ayvalık, (Balıkesir), Turkey. Ore Geol. Rev. 37, 175–201.
Oyman, T., Özgenç, İ., Tokçaer, M., Akbulut, M., 2013. Petrology, geochemistry, and evolution of the iron skarns along the northern contact ofthe Eğrigöz Plutonic Complex, western Anatolia, Turkey. Turk. J. Earth Sci. 2, 61–97.
Pearce, J.A., Harris, N.B.W., Tindle, A.G., 1984. Trace element discrimination diagram for the tectonic interpretation of granitic rocks. J. Petrol. 25, 956–983.
Pejatoviç, S., 1971. Doğu Karadeniz-Küçük Kafkasya Bölgesindeki Metalojenik Zonlar Ve Bunların Metalojenik Özellikleri. MTA Raporu, Ankara.
Ravna, E.K., 2000. The garnet ± clinopyroxene Fe^{2+}-Mg geothermometer: An updated calibration. J. metamorphic Geology 18, 211–219.
Ray, G.E., Dawson, G.L., Webster, I.C.L., 1996. The stratigraphy of the Nicola Group in the Hedley District, British Columbia, and the chemistry of its intrusions and Au skarns. Can. J. Earth Sci. 33, 1105–1126.
Ray, G.E., Webster, I.C.L., Ballantyne, S.B., Kilby, C.E., Cornelius, S.B., 2000. The geochemistry of three tin-bearing skarns and their related plutonic rocks, Atlin, Northern British Columnia. Econ. Geol. 95, 1349–1356.
Saraç, S., 2003. Doğu Karadeniz Bölgesi Demirli Skarn Yataklarının Karşılaştırmalı Mineralojik ve Jeokimyasal Özellikleri. Unpublished PhD. thesis Karadeniz Technical University, Fen Bilimleri Enstitüsü.
Saraç, S., Van, A., 2005. Comparative mimeralogical and chemical of Çambaşı (Ordu) and Dereli (Giresun) areas skarn deposits: Northern zones of Eastern Black Sea (NE Turkey). Jeoloji Mühendisliği Dergisi 29 (2), 27–44.
Şen, C., Arslan, M., Van, A., 1998. Geochemical and petrological characteristics of the eastern Pontide Eocene (?) Alkaline Volcanic Province, NE Turkey. Turk. J. Earth Sci. 7, 231–239.
Şengör, A.M.C., Yılmaz, Y., 1981. Tethyan evolution of Turkey: a plate tectonic approach. Techtonophysics 75, 181–241.
Şengör, A.M.C., Özeren, S., Genç, T., Zor, E., 2003. East Anatolian high plateau as a mantle-supported, north-south shortened domal structure. Geophys. Res. Lett. 30 (24), 1–4.
Singoyi, B., Zaw, K., 2001. A petrological and fluid inclusion study of magnetite-scheelite skarn mineralization at Kara, Northwestern Tasmania, Implications for Ore Genesis. Chem. Geol. 173, 239–253.
Sipahi, F., 2011. Formation of skarns at Gümüşhane (Northeastern Turkey). Neues Jb. Mineral. Abh. 188, 169–190.
Sipahi, F., Sadıklar, M.B., 2010. The alteration mineralogy and mass change of the Zigana (Gümüşhane) volcanic of NE Turkey. Geol. Bull. Turk. 53, 122–155.
Sipahi, F., Sadıklar, M.B., 2014. Geochemistry of dacitic volcanics in the Eastern Pontides (NE Turkey). Geochem. Int. 4, 329–349.
Sipahi, F., Sadıklar, M.B., Şen, C., 2014. The geochemical and Sr-Nd isotopic characteristics of Murgul (Artvin) volcanics in the eastern Black Sea region (NE Turkey). Chem. Erde-Geochem. 74, 331–342.
Sipahi, F., Saydam Eker, Ç., Kaygusuz, A., Vural, A., 2016. Investigation of mineral chemistry, fluid inclusion and stable isotope composition of skarn mineralization at Eğrikar (Torul-Gümüşhane, NE Turkey). In: Tübitak 3001 Project, No: 114Y013, Ankara, 182 p., Turkey.
Takaoğlu, S., Kanitani, W., Çekiç, Y., Şahinoğlu, 1978. Gümüşhane-Torul-Eğrikar Bakır-Demir Zuhurunun 1/10.000 Ölçekli Jeoloji Raporu. In: MTA Raporu, No: 4284.
Taylor, H.P., 1986. Magmatic volatiles: Isotopic variation of C, H, and S. Mineral. Soc. Am. 16, 185–225.
Tokel, S., 1977. Eocene calc-alkaline andesites and geotectonism in the Eastern Black Sea region. Türk. Jeol. Kurumu Bül. 20, 49–54.
Topuz, G., Altherr, R., Schwarz, W.H., Siebel, W., Satır, M., Dokuz, A., 2005. Postcollisional plutonism with adakite-like signatures: the Eocene Saraycık granodiorite (Eastern Pontides, Turkey). Contrib. Mineral. Petrol. 150, 441–455.
Topuz, G., Altherr, R., Schwarz, W.H., Dokuz, A., Meyer, H.P., 2007. Variscan amphibolite-facies rocks from the Kurtoğlu metamorphic complex. Gümüşhane area, Eastern Pontides, Turkey. Int. J. Earth Sci. 96, 861–873.
Ustaömer, T., Robertson, H.F.A., 2010. Late Paleozoic–Early Cenozoic tectonic development of the Eastern Pontides (Artvin area), Turkey: stages of closure of Tethys along the southern margin of Eurasia. Geol. Soc. Lond. Spec. Publ. 340, 281–327.
Valkama, M., Sundblad, K., Cook, N.J., Ivashchenko, V.I., 2016. Geochemistry and petrology of the indium-bearing polymetallic skarn ores at Pitkäranta, Ladoga Karelia, Russia. Mineral. Deposita. http://dx.doi.org/10.1007/s00126-016-0641-4.
Wiedenbeck, M., Alle, P., Corfu, F., Griffin, W.L., Meier, M., Oberli, F., Vonquadt, A., Roddick, J.C., Speigel, W., 1995. Three natural zircon standards for U–Th–Pb, Lu–Hf, trace-element and REE analyses. Geostand. Newslett. 19, 1–23.
Wilkinson, J., 2001. Fluid inclusions in hydrothermal ore deposits. Lithos 55, 229–272.
Xie, G., Mao, J., Zhu, Q., Yao, L., Li, Y., Li, W., Zhao, H., 2015. Geochemical constraints on Cu–Fe and Fe skarn deposits in the Edong district, Middle–Lower Yangtze River metallogenic belt, China. Ore Geol. Rev. 64, 425–444.
Xu, Y.M., Jiang, S.Y., Zhu, Z.Y., Zhou, W., 2015. Mineral chemistry and H–O–S–Pb

isotopic compositions of skarn type copper deposits in the Jiurui district of the Middle-Lower Yangtze River metallogenic belt, Eastern China. Ore Geol. Rev. 69, 88–103.
Yiğit, Ö., 2006. Gold in Turkey —a missing link in Tethyan metallogeny. Ore Geol. Rev. 28, 147–179.
Yiğit, Ö., 2009. Mineral deposits of Turkey in relation to Tethyan Metallogeny: implications for future mineral exploration. Econ. Geol. 104, 19–51.
Yılmaz, M., 2016. Eğrikar (Torul, Gümüşhane) Fe-Cu Skarn Cevherleşmesinin Petrografik ve Jeokimyasal Açıdan İncelenmesi. Unpublished M.Sc. thesis Fen Bilimleri Enstitüsü, Gümüşhane University.
Yılmaz, S., Boztuğ, D., 1996. Space and time relations of three plutonic phases in the Eastern Pontides, Turkey. Int. Geol. Rev. 38, 935–956.
Yılmaz, Y., Tüysüz, O., Yiğitbaş, E., Genç, Ş.C., Şengör, A.M.C., 1997. Geology and tectonic evolution of the Pontides. In: Robinson, A.G. (Ed.), Regional and Petroleum Geology of the Black Sea and Surrounding Region. American Association of Petroleum Geologists Memoir Vol. 68. pp. 183–226.
Yılmazer, E., 2012. Genetic Modeling of the Şamlı (Balıkesir) Iron Deposit. Unpublished PhD. thesis Naturel and Applied Sciences Enstitute, Middle East Technical University, Ankara.
Yılmazer, E., Güleç, N., Kuşcu, İ., Lentz, D.R., 2014. Geology, geochemistry, and geochronology of Fe-oxide Cu (± Au) mineralization associated with Şamlı pluton, western Turkey. Ore Geol. Rev. 57, 191–215.
Zaw, K., Singoyi, B., 2000. Formation of magnetite-scheelite skarn mineralization at Kara, northwestern Tasmania: evidence from mineral chemistry and stable isotopes. Econ. Geol. 95, 1215–1230.
Zhao, Y., Dong, Y., Li, D., Bi, C., 2003. Geology, minerology, geochemistry, and zonation of the Bajiazi dolostone-hosted Zn-Pb-Ag skarn deposit, Liaoning Province, China. Ore Geol. Rev. 23, 153–182.
Zheng, Y.F., 1993. Calculation of oxygen isotope fractionation in anhydrous silicate minerals. Geochim. Cosmochim. Acta 57, 1079–1091.
Zheng, Y.F., Hoefs, J., 1993. Carbon and oxygen isotopic covariations in hydrothermal calcite: Theoretical modeling on mixing processes and application to Pb-Zn deposits in the Harz Mountains, Germany. Mineral. Deposita 28, 79–89.
Zheng, Y.-F., Simon, K., 1991. Oxygen isotope fractionation in hematite and magnetite: a theoretical calculation and application to geothermometry of metamorphic iron-formations. Eur. J. Mineral. 3, 877–886.
Zürcher, L., Ruiz, J., Barton, M.D., 2001. Paragenesis, elemental distribution, and stable isotopes at the Pena Colorada iron skarn, Colima, Mexico. Econ. Geol. 96, 535–558.